An Estimate of the Isopycnal Diffusion Tensor Based on Particle Statistics.

by
Stefan Riha

Submitted to the faculty of the program
Climate Physics: Meteorology and Physical Oceanography
in partial fulfillment of the requirements for the degree of Masters of Science at

IFM-GEOMAR, Leibniz Institute of Marine Sciences (at Kiel University)

Supervisor: Carsten Eden

August 2009

Contents

1 Introduction **3**
1.1 Motivation 3
1.2 Taylor's Theory of Turbulent Dispersion 5
1.3 Turbulent Diffusivity and Lagrangian Particle Statistics 8
1.4 Anisotropy 16
1.5 Inferring Eddy Diffusivities from Oceanic Drifters: Strategy and Caveats. 17

2 Method **18**

3 Results **22**

4 Discussion **36**

Abstract

The quality of eddy flux-gradient parametrizations in models with coarse resolution depends on whether the generated diffusivity is similar to that of reference solutions produced by eddy resolving models. It is therefore essential to accurately describe the transport properties of eddy resolving ocean models. This thesis is a survey of the lateral transport of passive tracers induced by mesoscale eddies in the velocity field of a $1/12^o$ numerical model of the North Atlantic. Statistical tools are used to relate particle trajectories of Lagrangian floats to the effective eddy diffusivity: Both Taylor's theory of turbulent dispersion, which forms the foundation for the analysis, and further refinements thereof, are discussed and used for computations. The underlying theories rely on several restrictive assumptions about the statistics of the flow field, and one objective of this thesis is to make the reader aware of how difficult an interpretation of the results can be.

... Obviously, we must assume that each individual particle performs a motion that is independent of the motions of all the other particles; similarly, the motions of one and the same particle in different time intervals will have to be conceived as mutually independent processes so long as we think of these time intervals as chosen not to be too small....

Albert Einstein, 1905: On the Movement of Small Particles Suspended in Stationary Liquids Required by the Molecular-Kinetic Theory of Heat. *Annalen der Physik (ser. 4), 17, 549-560*

1 Introduction

1.1 Motivation

Predicting future distributions of tracers like dissolved oxygen, dissolved inorganic carbon or nitrate in the ocean is a central problem in climate research. Changes of the distribution are caused by the inital condition, by sources and sinks of the tracer and the evolution of the velocity field by which the tracers are transported. Ocean components of climate models are integrated for long time-intervals, and their spatial resolution is kept low to reduce the computational load. A model with coarse resolution cannot resolve features of the velocity field which are present in the real ocean, or in a model with finer resolution, and this is why a coarse resolution model predicts different tracer distributions than a model with finer resolution. The coarse resolution model is nevertheless considered to be useful, if it represents an average of multiple individual results produced with the fine resolution model [1]. It is therefore desireable to design a coarse model in a way that it reproduces the *average effect* of the unresolved features of velocity onto the transport of tracers.
The flow by which a tracer is advected in the ocean has very different dynamical properties in the along- and cross-isopycnal directions (Garrett, 1983); While tracer distributions in the cross-isopycnal direction appear smooth on scales of more than a few meters, variations in the along-isopycnal direction can be observed at much larger scales. The variability on the lowest frequencies and the largest spatial scales which cannot be resolved by climate models is caused by a variety of mesoscale structures; jets, intense vortices, eddies and planetary waves (Berloff & McWilliams, 2002). Apart from the mean currents, the dominant transport mechanism along isopycnals is associated with stirring by mesoscale eddies (Garrett, 2006). Dispersion caused by eddies affects the evolution of large-scale patterns of every tracer; active scalar tracers like temperature and salt, passive tracers like dissolved oxygen, dissolved inorganic carbon or nitrate, as well as dynamical quantities like potential vorticity. Most ocean components of climate models cannot resolve mesoscale eddies.
With this work we aim to improve simple eddy-diffusivity parameterizations of isopycnal dispersion for coarse resolution ocean models by inferring appropriate eddy-diffusivity constants from the flow field of an eddy-permitting model of the North Atlantic. Diffusivity constants represent a growth

[1] The results of the individual simulations with the fine resolution model might differ because of small changes in the initial conditions.

rate of variance of the tracer field, and we choose to analyze the dispersal of Lagrangian particles in the eddy-permitting model to calcualte an appropriate growth rate.
It was mentioned above that a successful parameterization of turbulent fluxes should represent the average transport effect of unresolved velocity fluctuations. It is therefore interesting to think about how the average result of a tracer release experiment differs from an individual result.
Stages of tracer dispersal as observed in an individual tracer-release experiment. Garrett (2006) and Lee *et al.* (2009) identify various distinct stages of tracer dispersal in an individual tracer release experiment. The numbers below are estimates and represent typical oceanic values. Let us assume that a patch of tracer substance with diameter of about 1m is instantaneously released in the ocean and that the patch lies on an isopycnal.

- **Stage 1**: Processes like shear dispersion of inertial and internal waves cause a dispersal of the tracer along isopycnals, and dispersal across isopycnals is caused by processes such as breaking of internal waves. These mechanisms act on scales of the order of 1-100m and they are directly linked to mixing at the molecular level.

- **Stage 2**: The tracer patch is gradually deformed such that it extends over a distance of more than about 100m. At this time it will start to be distorted and strained into streaks by mesoscale eddies. This process is commonly referred to as *stirring*. In this stage, the evolution of the tracer patch is dominated by the local strain field rather than by the small-scale processes mentioned above. The stirring process is adiabatic with the tracer contours stretched and gradients sharpened. This enhances molecular diffusion. While the patch is distorted, the center of mass of the tracer patch will move away from the location of release. From now on, the deformation of the tracer patch can be observed by seeding neutrally buoyant floats along the tracer contours.

- **Stage 3**: When the length scale of the tracer is much larger than the typical eddy size, streaks of tracer are repeatedly elongated, folded and eventually merged together by diffusion. This leads to a smoothing, or reduction of streakiness. After some time, variations of concentration have a spatial extent on the order of the length scale of the dominant eddies.

Consider the shape of a tracer contour (in two dimensions this would be a path along which the concentration is constant) and its evolution in time. When the tracer is released this contour will have the form of a circle, which will be strongly distorted by the eddies at stage 2. An ocean model with coarse resolution is not able to reproduce this kind of streakiness; The length scale of the streaks is about the same as the length scale of the eddies, which cannot be resolved with coarse resolution.
Evolution of the ensemble-mean distribution. If the experiment outlined above is repeated many times, the individual shapes of distributions can be averaged. In this work we try to extract information about the evolution of the ensemble-mean distribution at times after stage 3 reached its final phase: The extent of the ensemble-mean tracer distribution has grown so large that deviations from the ensemble mean are on the order of the length scale of the dominant eddies times the mean gradient of concentration (Davis, 1991). Davis (1987) emphasizes that it is fundamentally incorrect to confuse the average effects of eddies onto the evolution of a tracer field with the kind of stirring outlined above in stage 2. Imagine a turbulent flow (A) that produces very elongated streaks during stage 2 in every individual realization, and moves the center of gravity away from its initial position. Consider a different kind of turbulent flow (B) in which the center of gravity of the tracer patch is moved in the same way as in flow A, but in which the velocity fluctuations distort the patch only slightly and do not lead to elongated streaks as before. In principle, both kinds of turbulence can lead to an identical ensemble-mean evolution of the tracer patch, because the different characteristics dissappear in the averaging process. However, Garrett (1983) argues that the distinction between

the ensemble averaged concentration field and the potentially streaky concentration field in a single realization may not be important if the tracer concentrations are low.
The method we employ is based on the fact that the evolution of the ensemble-mean tracer field is fully determined by single-particle statistics (Davis, 1987). Single-particle statistics do not yield information about the degree to which individual tracer patches are distorted in stage 2. As the name suggests, single-particle statistics are computed from an ensemble of releases of one particle per experiment. Instead of repeating the experiment, we assume that the eddy-permitting model produces stationary fluctuation-statistics and imagine that a new experiment starts each time a particle passes the point of release.
This approach is to be distinguished from the one used by Lee *et al.* (2009), who apply diagnostic methods to infer eddy diffusivity from a single point release [2] of a chemical tracer in a numerical model. The authors note that the relationship betwen different methods of inferring diffusivity is often not clear, which makes it difficult to interpret the meaning of eddy diffusivity. They find that the time scales associated with the final stage of tracer evolution is different for each method.
The use of floats as opposed to chemical tracers provides an economical way of obtaining information on material transport in the real ocean.
The rest of this chapter is divided into four parts: The first part is an outline of Taylor's theory of turbulent dispersion. This theory will be used in the second part to explain what Lagrangian particle statistics have to do with turbulent diffusion. The third part explaines the concept of anisotropic diffusion, and the fourth part outlines some problems relating to the statistical sampling of the ocean or an ocean model.

1.2 Taylor's Theory of Turbulent Dispersion

If a set of particles is released at a point into a turbulent fluid, the particles will be advected by the large-scale mean flow and by the turbulent velocity fluctuations. In this section we consider only the part of the transport which is caused by turbulent velocity fluctuations. To this end we assume that the mean flow vanishes. Recall that the ultimate goal of this work is to find parameterizations of turbulent fluxes which represent the average transport effect of unresolved velocity fluctuations. The effects of turbulence onto changes of the distribution of a tracer are of course dependent on its initial distribution. In this section we consider the dispersal of particles which are released at one single point. An important characteristic of the average transport effect is the mean square distance between the point of release and the location of a particle. It will become clear that this mean square distance grows with time, but this is rather trivial. Further analysis show that shortly after release, the mean square distance will grow faster than linear, but at some later time it will grow linearly in time. The length of the time intervall after which the mean square displacement grows linearly depends on the nature of the turbulence. One way of characterizing the nature of a specific kind of turbulence with Lagrangian statistics is to calculate the velocity-autocorrelation function of Lagrangian particles which are advected by the turbulent velocity; Different regimes of turbulence will cause different shapes of velocity-autocorrelation functions. The length of the time intervall after which the mean square displacement grows linearly in time depends strongly on the shapes of the velocity-autocorrelation functions.
A turbulent flow is called *quasi-stationary* if the statistics of the turbulent fluctuations are independent of space. Likewise, it is called *homogeneous* if the statistics of the fluctuations are independent of time. The distinction of the two properties (quasi-stationarity and homogeneity) can only be made from the perspective of an Eulerian description of the flow. In the Lagrangian frame, location is a function of time. If a Lagrangian particle is released in a quasi-stationary, but nonhomogeneous flow, it will change its position with time and sample various regions that are characterized by different Eulerian statistics. The time series of the particle's velocity is thus a realization of a

[2] No ensemble averaging is involved.

non-stationary stochastic process. Even if the Eulerian statistics are quasi-stationary and homogeneous in the horizontal direction, the Lagrangian statistics of the horzontal velocity may not be stationary. The example of the Stokes Drift in wave fields illustrates this problem (Davis, 1991). Consider a wave field that is quasi-stationary and homogeneous in the horizontal directions. If Lagrangian particles are released at random times on the same point in the domain, their ensemble average velocity at the time of release will be zero, like the Eulerian mean velocity at this point. However, the nonlinearity of the flow will induce a Lagrangian mean velocity of the particle. For the development of the theory below, it is assumed that the timeseries of the velocity of a particle is a stationary process[3].

Consider a fluid with turbulent velocity fluctuations. A particle is released into the fluid, at the origin of coordinates, and advected by the turbulent fluctuations. Let $\mathbf{X}(t)$ be the position of the particle at time t. If the experiment can be repeated, we can obtain the ensemble mean position $\overline{\mathbf{X}}(t)$ of the particles.

In the following, the theory is developed according to Kundu & Cohen (2002).

It is sufficient to consider a single component of the displacement, e.g. X. The other components are treated in an analogous manner. The rate at which the mean square displacement $\overline{X^2}$ increases is

$$\frac{d}{dt}\left(\overline{X^2}\right) = 2\overline{X\frac{dX}{dt}}, \tag{1}$$

where $\frac{dX}{dt}$ is the Lagrangian velocity component of a particle. The bar $\overline{}$ denotes the ensemble mean, so the average is constructed by an infinite number of repetitions of the experiment. For further development let the Lagrangian velocity be defined by

$$u_l := \frac{dX}{dt}. \tag{2}$$

The particle position X can now be written in terms of its velocity history,

$$X(t) = \int_0^t u_l(t')\,dt', \tag{3}$$

which yields for (1):

$$\frac{d}{dt}\left(\overline{X^2}\right) = 2\overline{Xu_l} = 2\overline{\left[\int_0^t u_l(t')\,dt'\right]u_l(t)} \tag{4}$$

The instantaneous velocity u_l is a function of t and it is independent of t'. We can therefore put it into the integral:

$$\frac{d}{dt}\left(\overline{X^2}\right) = 2\overline{Xu_l} = 2\overline{\int_0^t u_l(t')u_l(t)\,dt'} \tag{5}$$

The operation of integration commutes with ensemble averaging, because

$$\overline{\int_0^t a(t')\,dt'} = \frac{1}{N}\left[\int_0^t a^1(t')\,dt' + \int_0^t a^2(t')\,dt' + \int_0^t a^3(t')\,dt' + \ldots\right] = \tag{6}$$
$$\int_0^t \left[\frac{1}{N}\left\{a^1(t') + a^2(t') + a^3(t') + \ldots\right\}\right]\,dt' = \int_0^t \overline{a(t')}\,dt',$$

[3]In fact, we assume that it is an ergodic process. Although not every stationary process is ergodic, a distinction between these two properties is not necessary in this context.

where the a^i are individual realizations of a. For (5) we get

$$\frac{d}{dt}\left(\overline{X^2}\right) = 2\int_0^t \overline{u_l(t')u_l(t)}\,dt' \tag{7}$$

We postulated that the particle's velocity is the realization of a stationary process, which implies that the expression $\overline{u_l(t')u_l(t)}$ is a function of the time difference $t - t'$ only. We can define the (normalized) autocorrelation function

$$r(\tau) = \frac{\overline{u_l(t)u_l(t+\tau)}}{\overline{u_l^2}}. \tag{8}$$

Note that $\overline{u_l^2}\, r(t'-t) = \overline{u_l(t)u_l(t')}$. By setting $\tau = t - t'$ we can rewrite (7) as

$$\frac{d}{dt}\left(\overline{X^2}\right) = 2\overline{u_l^2}\int_0^t r(\tau)\,d\tau \tag{9}$$

Integration yields

$$\overline{X^2}(t) = 2\overline{u_l^2}\int_0^t\int_0^{t'} r(\tau)\,d\tau\,dt'. \tag{10}$$

The last equation can be integrated by parts:

$$\begin{aligned}\overline{X^2}(t) &= 2\overline{u_l^2}\left(\left[t'\int_0^{t'} r(\tau)\,d\tau\right]_0^t - \int_0^t t' r(t')\,dt'\right) \\ &= 2\overline{u_l^2}\left(t\int_0^t r(\tau)\,d\tau - \int_0^t t' r(t')\,dt'\right) = 2\overline{u_l^2}t\int_0^t \left(1-\frac{\tau}{t}\right) r(\tau)\,d\tau\end{aligned} \tag{11}$$

The shape of the autocorrelation function will differ for various types of turbulence, but all autocorrelation functions share the following property:

- $r(0) = 1$. This follows from the definition (8).

Furthermore it may be assumed that most autocorrelation functions of turbulent flow satisfy:

- $\lim_{\tau\to\infty} r(\tau) = 0$. The velocity of a particle will become uncorrelated with itself after a long time.

If $r(\tau)$ converges fast enough to its limit at infinity, the integral

$$T_L = \int_0^\infty r(\tau)\,d\tau \tag{12}$$

converges and we can define T_L to be the Lagrangian integral time scale. In the literature, T_L sometimes appears as a measure of the time over which u_l stays highly correlated with itself. It is important to note that this interpretation of T_L is not always appropriate. We will discuss this issue below.
Depending on the shape of r close to the origin, we can find a t_a such that

$$r(t) \approx 1 \qquad \text{for} \quad t \le t_a \tag{13}$$

For $t \le t_a$, Eq. (1.2) can be approximated by

$$\overline{X^2}(t) = 2\overline{u_l^2}t\int_0^t \left(1-\frac{\tau}{t}\right)\,d\tau = \overline{u_l^2}t^2 \qquad t \le t_a. \tag{14}$$

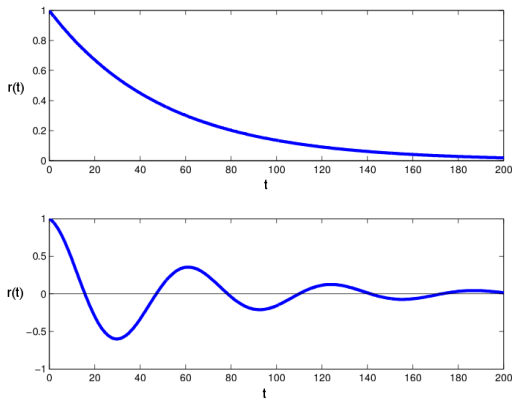

Figure 1: Two examples for autocorrelation functions.

This is as expected: Short after release, a particle's typical excursion is its rms speed multiplied by the time that has passed since its release (Garrett, 2006).

Depending on the speed of convergence of

$$T_L = \int_0^\infty r(\tau)\, d\tau, \tag{15}$$

we can find a t_b such that

$$T_L \approx \int_0^{t_b} r(\tau)\, d\tau, \tag{16}$$

For $t \geq t_b$, Eq. (1.2) can be approximated by

$$\overline{X^2}(t) = 2\overline{u_l^2} t \int_0^t r(\tau)\, d\tau = 2\overline{u_l^2} T_L t. \tag{17}$$

The mean square displacement grows linearly in time. Consider the two (artificially constructed) autocorrelation functions in Fig. 1. Both functions are close to zero after a lag of 200, so $t_b \approx 200$. However, $T_L \approx 50$ for the upper curve, and $T_L \approx 2$ for the lower curve. In the latter case it is clearly inappropriate to interpret T_L as a decorrelation time scale.

1.3 Turbulent Diffusivity and Lagrangian Particle Statistics

Recall that the goal of this work is to find parameterizations of turbulent fluxes which represent the average transport effect of unresolved velocity fluctuations. A change in concentration at a point during a time interval $[t_1, t_2]$ due to the average effect of turbulent transport is dependent on the tracer distribution at time t_1 and the probabilities of particle displacement from the surrounding points to the point under consideration. We are interested in finding, for every point x in the domain, the probability that particles move from any other point $\hat{x}$ to x during $[t_1, t_2]$. In the preceeding section we described Taylor's thought experiment and outlined the necessary assumptions about the turbulent velocity field. It was shown that the mean square distance between the point of release and the location of a particle grows with time. Taylor's theory does not predict the shape of the location probability distribution, it merely predicts its variance. The fact that the mean square displacement grows linearly after some time t_b (which depends on the nature of the turbulence) motivates the attempt to use an analog of the mathematical model of molecular diffusion for describing turbulent dispersion. In the next paragraph we explain some properties of the diffusion equation which are

relevant to eddy diffusivity modeling, and proceed to outline the basic ideas behind the concept of eddy diffusivity.

The diffusion equation. The diffusion equation is a mathematical model that describes the spreading of a conserved quantity like molecules, heat or momentum. The spreading is driven by spatial gradients of the quantity. Molecular diffusion is associated with a transfer of mass, while diffusion of heat is a transfer of thermal energy and diffusion of momentum refers to the spreading of momentum between particles. In any case, diffusion is a specific form of transport that is conceptually associated with randomness and irreversibility. Consider the example of dispersion of molecules in a fluid that is caused by their random[4] thermal agitation. A mathematical model for a simple case of a spreading process is formulated with the following initial value problem:

$$\frac{\partial C}{\partial t} = \kappa_{mol} \frac{\partial^2 C}{\partial x^2}, \qquad -\infty < x < \infty, \qquad 0 < t < \infty \tag{18}$$

$$C(x, 0) = \delta(x) \tag{19}$$

This is a model for molecular diffusion of a substance that is released at a point $x = 0$ in an unbounded, one-dimensional domain. The total amount of substance is one unit of mass. Initially, the concentration C is nonzero only at the point of release, which is expressed by the use of the Dirac-δ function in the initial condition. The solution to the initial value problem is given by

$$C(x, t) = \frac{1}{\sqrt{4\pi k_{mol} t}} \exp^{-\frac{x^2}{4k_{mol}t}} \tag{20}$$

At every time t_i, the solution is identical to a Normal distribution

$$\frac{1}{\sigma\sqrt{2\pi}} \exp^{-\frac{(x-\mu)^2}{2\sigma^2}} \tag{21}$$

with $\mu = 0$ and $\sigma^2 = 2k_{mol}t_i$ The evolution of the concentration C is expressed by the linear increase of variance of a Gaussian shape. The Normal distribution describes the probability density function of the position of a molecule of the released substance. The variance $\sigma^2 = 2k_{mol}t$ is equal to the mean square displacement of the molecules from the point of release. Transport by means of diffusion is caused by random movements, which is consistent with the fact that the solution of the diffusion equation has the shape of a probability density function at every instant. The diffusion equation does not predict the location of a molecule, it merely assigns a probability of finding it at a certain point. The increase in variance is the result of growing uncertainty in the position of molecules and it is this growing unpredictability which introduces the irreversible nature of diffusion (adapted from Davis (1987)).

The advection equation. A simple form of the advection equation is

$$\frac{\partial C}{\partial t} + u\frac{\partial C}{\partial x} = 0. \tag{22}$$

The equation models the transport of a conserved quantity which is caused by a fluid that moves with the velocity u. As opposed to diffusion, this kind of transport is not influenced by randomness, but it is determined by the velocity of the fluid.

Turbulent transport: Reynolds averaging of the advection equation. In a numerical ocean model, the velocity field cannot be resolved to small scales at which viscosity becomes relevant. The velocity and the tracer field are decomposed into average fields $\overline{u}, C$ and a part which represents turbulent fluctuations u', C'. The decomposition $u = \overline{u} + u'$ is called *Reynolds decomposition* and

[4]We call a process *random*, if it is either random or chaotic. Although the two words have different meanings, a proper distinction is beyond the scope of this work. We assume that ensembles of both random and chaotic processes can be described by a probability density functions after a certain time interval.

the averaging can be done in various ways. In any case, for a turbulent flow the fluctuations u' and c' are considered to be *random* and can be described, if at all, by a probability density function. Inserting the Reynolds averaged quantities in equation (22) yields

$$\frac{\partial C}{\partial t} + \overline{u}\frac{\partial C}{\partial x} = -\frac{\overline{\partial u'C'}}{\partial x}. \tag{23}$$

The second term on the left hand side represents advection by the velocity at scales that can be resolved by the model, while the term on the right hand side models the contributions of random fluctuations to the evolution of the mean fields.

Parameterization of the turbulent flux. The turbulent flux $\overline{u'C'}$ must be expressed as a function of the mean variables. In a flow with zero mean velocity, (23) reduces to

$$\frac{\partial C}{\partial t} = -\frac{\overline{\partial u'C'}}{\partial x}. \tag{24}$$

Taylor (1922) showed that, under the restrictions outlined in 1.2, the mean square displacement of an ensemble of particles released in a turbulent fluid is a linear function of time, provided that $t \geq t_b$. Recall that

$$\left(\overline{X_1^2}\right) = 2\overline{u_l^2}T_L t \qquad \text{for} \quad t \geq t_b, \tag{25}$$

where t_b is the time of decorrelation for a velocity fluctuation. The increase of variance of the location uncertainty is therefore a linear function of time, just like it was in the case of molecular diffusion. This fact is a key argument for justifying eddy diffusivity modeling. In eddy diffusivity modeling, the probability of finding a particle at a certain location is expressed by substitution of k_{mol} in (19) with $\overline{u_l^2}T_L$.

$$\frac{\partial C}{\partial t} = \overline{u_l^2}T_L\frac{\partial^2 C}{\partial x^2}, \tag{26}$$

This is a simple flux-gradient parameterization: The term $-\overline{u'C'}$ in (24) is substituted with $\overline{u_l^2}T_L\frac{\partial C}{\partial x}$. Extending this idea to flows with a spatially constant mean velocity, (23) can be written as an advection-diffusion equation:

$$\frac{\partial C}{\partial t} + u\frac{\partial C}{\partial x} = \kappa\frac{\partial^2 C}{\partial x^2} \qquad \kappa := \overline{u_l^2}T_L \tag{27}$$

Mapping of Lagrangian statistics into an Eulerian frame. It is essential to note that Eq. (27) is written in an *Eulerian* frame and contains a *Lagrangian* statistic $u_l^2 T_L$. With the assumptions of section 1.2, the turbulent diffusivity $\overline{u_l^2}T_L$, a statistic that must be computed from particle displacements and therefore can not be computed at a single point, is nevertheless representative for every point in the entire spatial and temporal domain.

Towards a more advanced justification for the use of (27)**.** Taylor's theory describes the spreading of particles that are released from a concentrated point source in an idealized turbulent flow with zero mean flow. A thorough discussion about the applicability of (27) in general circulation models is beyond the scope of this work. However, we can strengthen our intuition by trying to understand the appendix of the article by Davis (1987). The description of molekular diffusion from the microscopic (as opposed to the continuous) perspective goes back to Einstein (1905). Further information is available in Davis (1983) and Davis (1991).

In the following we use the notation $a(t|\tilde{x},\tilde{t})$ to denote the property a at time t of a particle which was found (or will be found) at the Eulerian space-time coordinate $(\tilde{x},\tilde{t})$. The coordinates behind the bar are sometimes referred to as *Lagrangian label*. Note that every moving particle has an infinite

amount of labels, i.e. all Eulerian coordinates which lie on its trajectory can be used to identify the particle in an unambiguous way.
The advection equation (22) can be written as

$$\frac{dc}{dt} = 0, \tag{28}$$

where $\frac{d}{dt}$ is the total derivative of c. Assume that we know the initial concentration $c(x,0)$. The solution to the advection equation is given by

$$c(x,t) = c\{r(0|x,t),0\} = \int \delta\{\tilde{x} - r(0|x,t)\}c(\tilde{x},0)\,d\tilde{x}, \tag{29}$$

where r is the initial position of a particle (or 'blob of fluid') that is found at (x,t). The blob of fluid at (x,t) simply transported the c-stuff contained in it from its initial position to x during the time interval $[0,t]$. The integral in the above equation extends over the complete spatial domain. If we apply the ensemble average operator $\overline{}$ to the upper equation and assume that the fluid motion is independent of the initial distribution $c(x,0)$, we have

$$C(x,t) = \int P(x,[0,t],\tilde{x})C(\tilde{x},0)\,d\tilde{x}, \tag{30}$$

with

$$P(x,[0,t],\tilde{x}) = \overline{\delta\{\tilde{x} - r(0|x,t)\}} \tag{31}$$

$$C(\tilde{x},0) = \overline{c(\tilde{x},0)}. \tag{32}$$

$P(x,[0,t],\tilde{x})$ is the transition probability, i.e. the probability that a particle which was found at $(\tilde{x},0)$ moves to the point (x,t) during $[0,t]$.

Assume that there exists a time-interval Δ, such that

$$P(x,[0,t+\Delta],\tilde{x}) = \int P(\hat{x},[0,t],\tilde{x}) \cdot P(x,[t,t+\Delta],\hat{x})\,d\hat{x} \tag{33}$$

This important step introduces the conjecture that the time-domain can be split up into intervals for which the transition probabilities P are statistically independent from each other. The product $P(\hat{x},[0,t],\tilde{x}) \cdot P(x,[t,t+\Delta],\hat{x})$ is then the probability that a particle moves from $\tilde{x}$ to an arbitrary $\hat{x}$ during $[0,t]$, under the condition that it moves afterwards from $\hat{x}$ to x. (33) is equivalent to the assumption that sequential particle displacements which are temporally separated by Δ are effectively statistically independent, which implies that the transport is a first-order Markov process in the sense that the particle motion over the interval $[t,t+\Delta]$ depends statistically only on particle positions at t (Davis, 1987). From the assumption follows

$$\begin{aligned} C(x,t+\Delta) &= \int P(x,[0,t+\Delta],\tilde{x}) \cdot C(\tilde{x},0)\,d\tilde{x} = \\ &\int \left[\int P(\hat{x},[0,t],\tilde{x}) \cdot P(x,[t,t+\Delta],\hat{x})\,d\hat{x}\right] C(\tilde{x},0)\,d\tilde{x} = \\ &\int P(x,[t,t+\Delta],\hat{x}) \left[\int P(\hat{x},[0,t],\tilde{x}) \cdot C(\tilde{x},0)\,d\tilde{x}\right] d\hat{x} = \\ &\int P(x,[t,t+\Delta],\hat{x}) \cdot C(\hat{x},t)\,d\hat{x}. \end{aligned} \tag{34}$$

Further development involves assumptions about the shape of P with respect to the spatial arguments x and $\hat{x}$.

Assume that $P(x,[t,t+\Delta],\hat{x})$ is almost zero outside of an ϵ-neighborhood centered at x. Assume furthermore that C is well approximated within that neighborhood by a Taylor series expansion about x up to second order:

$$C(\hat{x},t) = C(x,t) + \frac{\partial C(x,t)}{\partial x}(\hat{x}-x) + \frac{1}{2}\frac{\partial^2 C(x,t)}{\partial x^2}(\hat{x}-x)^2 + O((\hat{x}-x)^3) \tag{35}$$

$$C(\hat{x},t) \approx C(x,t) + \frac{\partial C(x,t)}{\partial x}(\hat{x}-x) + \frac{1}{2}\frac{\partial^2 C(x,t)}{\partial x^2}(\hat{x}-x)^2 \qquad \text{for} \quad |\hat{x}-x| < \epsilon \tag{36}$$

Then

$$C(x,t+\Delta) \approx \int C(x,\Delta,\hat{x}) \left[C(x,t) + \frac{\partial C}{\partial x}(\hat{x}-x) + \frac{1}{2}\frac{\partial^2 C}{\partial x^2}(\hat{x}-x)^2 \right] d\hat{x} \tag{37}$$

The terms on the right hand side are

$$\int C(x,\Delta,\hat{x}) C(x,t)\, d\hat{x} = \int C(x,\Delta,\hat{x})\, d\hat{x} \cdot C(x,t) = C(x,t) \tag{38}$$

$$\int C(x,\Delta,\hat{x}) \frac{\partial C}{\partial x}(\hat{x}-x)\, d\hat{x} = -\int C(x,\Delta,\hat{x})(x-\hat{x})\, d\hat{x} \cdot \frac{\partial C}{\partial x} \tag{39}$$

$\int C(x,\Delta,\hat{x})(x-\hat{x})\, d\hat{x}$ is the expected value of the displacement vector pointing from the location $r(-\Delta|x,t)$ of a particle at time $-\Delta$ to the location x at time t. It also is the mean displacement of those particles which arrive at x during the time $[t-\Delta,t]$. Let's denote the mean displacement with $D(\Delta|x)$. Then (39) can be written as

$$-\int C(x,\Delta,\hat{x}) \frac{\partial C}{\partial x}(x-\hat{x})\, d\hat{x} = -D(\Delta|x)\frac{\partial C}{\partial x} \tag{40}$$

Consider now the last term in (37),

$$\int C(x,\Delta,\hat{x}) \frac{1}{2}\frac{\partial^2 C}{\partial x^2}(\hat{x}-x)^2\, d\hat{x} = \frac{1}{2}\int C(x,\Delta,\hat{x})(\hat{x}-x)^2\, d\hat{x} \cdot \frac{\partial^2 C}{\partial x^2}. \tag{41}$$

Let's denote the mean square displacement $\int C(x,\Delta,\hat{x})(\hat{x}-x)^2\, d\hat{x}$ with $D^2(\Delta|x)$. Then (37) can be written as

$$C(x,t+\Delta) = C(x,t) - D(\Delta|x)\frac{\partial C}{\partial x} + \frac{D^2(\Delta|x)}{2}\frac{\partial^2 C}{\partial x^2} \tag{42}$$

or

$$\frac{C(x,t+\Delta)-C(x,t)}{\Delta} + \frac{D(\Delta|x)}{\Delta}\frac{\partial C}{\partial x} = \frac{D^2(\Delta|x)}{2\Delta}\frac{\partial^2 C}{\partial x^2} \tag{43}$$

The last equation can be interpreted as an analog to the advection-diffusion equation for finite timescales. Note that Eq. (A.4) in Davis (1987) is identical to (43) only in the case where no sources or sinks are present and where D^2 is spatially invariant. The term $\frac{D(\Delta|x)}{\Delta}$, which can be interpreted as a mean velocity, is the *mean particle velocity*, not the Eulerian mean velocity appearing in (27). Despite the differences between (43) and the advection-diffusion equation, it is instructive to recall the premises under which it was derived.
(43) can only be accurate if two conditions are fulfilled:

1. Δ is large enough to guarantee that the process is Markovian.

2. Δ is small enough to yield sufficiently short particle displacements ($\hat{x} - x$), so that the Taylor series approximation (36) is accurate.

According to Davis (1987), Δ has to be much larger than the time scale of the Lagrangian covariance T_L. The flux-gradient parameterization in Eq. (27) can only be useful if the change of concentration depends only on the present value of concentration, i.e. the average particle motion over the time step Δ depends statistically only on particle positions at its start. If Δ is not large compared to T_L, then the processes of small-scale transport cannot be viewed as being constant during the time increment Δ. In this case, the 'nature' of small scale transport evolves during Δ. Davis (1987) generalizes Eq. (27) and derives an equation which is, in its finite difference approximation, valid for arbitrarily small time-increments Δ.

The mixing length scale: Mixing by large eddies. The mixing length approach leads to a parameterization of turbulent Reynolds stresses in the momentum equations. The formalism cannot be derived from fundamental physical principles, it rather is a formal description of empirical observations. In the remaining part of this section we outline why it may be useful to adopt the concept of a mixing length scale for tracer flux parameterizations, and we explain how Lagrangian particle statistics have been linked to the mixing length scale in the literature.

In the final stage of tracer dispersal (see Sec. 1), deviations from the ensemble mean are on the order of the length scale of the dominant eddies times the mean gradient of concentration. Consider a mean tracer field C, for which a turbulent fluctuation at the point x_0 is expressed as

$$C'(x_0, t) = -l \frac{\partial C(x_0, t)}{\partial x}, \tag{44}$$

where l is a vector pointing from a previous position of the particle to x_0. Formally, there always exists an l such that (44) holds, provided that $\frac{\partial C(x_0,t)}{\partial x} \neq 0$. However, mixing length theory teaches that (44) only leads to useful parameterizations as long as l is much smaller than the scales at which C varies. We anticipate that if Lagrangian particle statistics are used to back up the idea of a mixing length scale, this restriction will follow from the assumptions leading to (36). Using (44), the turbulent tracer flux is

$$\overline{u'C'}(x_0, t) = -\overline{u'l} \frac{\partial C(x_0, t)}{\partial x}. \tag{45}$$

Extension of (27) to weakly inhomogeneous flows. Davis (1987) argues that the concept of mapping Lagrangian statistics into an Eulerian frame can be extended to weakly inhomogeneous flows. Recall that (27) contains a single Lagrangian statistic that describes the growth of tracer variance at all points in the domain. In the case of inhomogeneous turbulence, the statistics of the turbulent fluctuations vary in space, and so κ must also vary in space:

$$\frac{\partial C}{\partial t} + u \frac{\partial C}{\partial x} = \frac{\partial}{\partial x} \left(\kappa(x) \frac{\partial C}{\partial x} \right). \tag{46}$$

Davis (1987) suggests to use

$$\kappa(x_0) = -\left(\overline{u'(x_0, t) \int_{-\infty}^{0} u_l'(t + \tau | x_0, t)\, d\tau} \right). \tag{47}$$

Compare this with the purely Lagrangian statistic $-\overline{u_l^2} T_L$ in (27):

$$\kappa = -\overline{u_l'^2} T_L = -\left(\overline{u_l'(t) \int_{0}^{\infty} u_l'(t + \tau)\, d\tau} \right) \tag{48}$$

The point here is that κ in (47) is still a Lagrangian statistic, but it can be mapped to a point in space, which is generally not the case for Lagrangian statistics.
The variable $\kappa(x_0)$ can be computed from an ensemble of individual particles passing through the point (x_0, t_0) (see Sec. 1.5), and this is why it is called a *single-particle statistic*. The limits of integration in (47) indicate that it is relevant where the particles arriving at (x_0, t_0) came from. To calculate the spatial variation of $\kappa(x)$, the complete spatial domain can be divided into subregions. Let the centers of the subregions be denoted by $(x_0, x_1, \ldots)$. Assume that the degree of inhomogeneity in the domain is such that each subregion is characterized by approximately constant fluctuation statistics. Then the statistic (47) can be computed for each point $(x_0, x_1, \ldots)$, and it will be representative for the subregion provided that particle displacements are contained within the subregion long enough so that the integrand of (47) is close to zero outside the subregion. Note that this assumption is necessary, otherwise the limits of integration in (47) do not make sense: u_l will not be defined at times prior to initialization, but the integrand $\overline{u'(x_0,t_0)u_l'(t)}$ is assumed to vanish at some point between initialization and t_0.
At this point it is interesting to look at (47) from the perspective of the mixing length approach:

$$\overline{u' \int_{-\infty}^{t} u_l'(t+\tau|x_0,t)\,dt} \quad \leftrightsquigarrow \quad \overline{u'l} \tag{49}$$

Let the vector pointing from the position $r(t_0 - t_b|x_0, t)$ to (x_0, t) of a particle causing a velocity perturbation $u'(x_0, t)$ be denoted by l. Recall that t_b is the time that a particle's velocity typically stays correlated with itself. Assume that the velocity fluctuation has been observed, but l is unknown. Davis (1987) shows that, under certain restrictive assumptions, l is optimally predicted by

$$l \quad \leftrightsquigarrow \quad \frac{\overline{u' \int_{-\infty}^{t} u_l'(t+\tau|x_0,t)\,dt}}{u'}. \tag{50}$$

A detailed outline of the necessary assumptions is given in Davis (1987).
To conclude this section, we present a simple flow-chart in Fig. 2. The chart is a (somewhat naive) answer to the question: *When can we use eddy diffusivity in ocean models?*

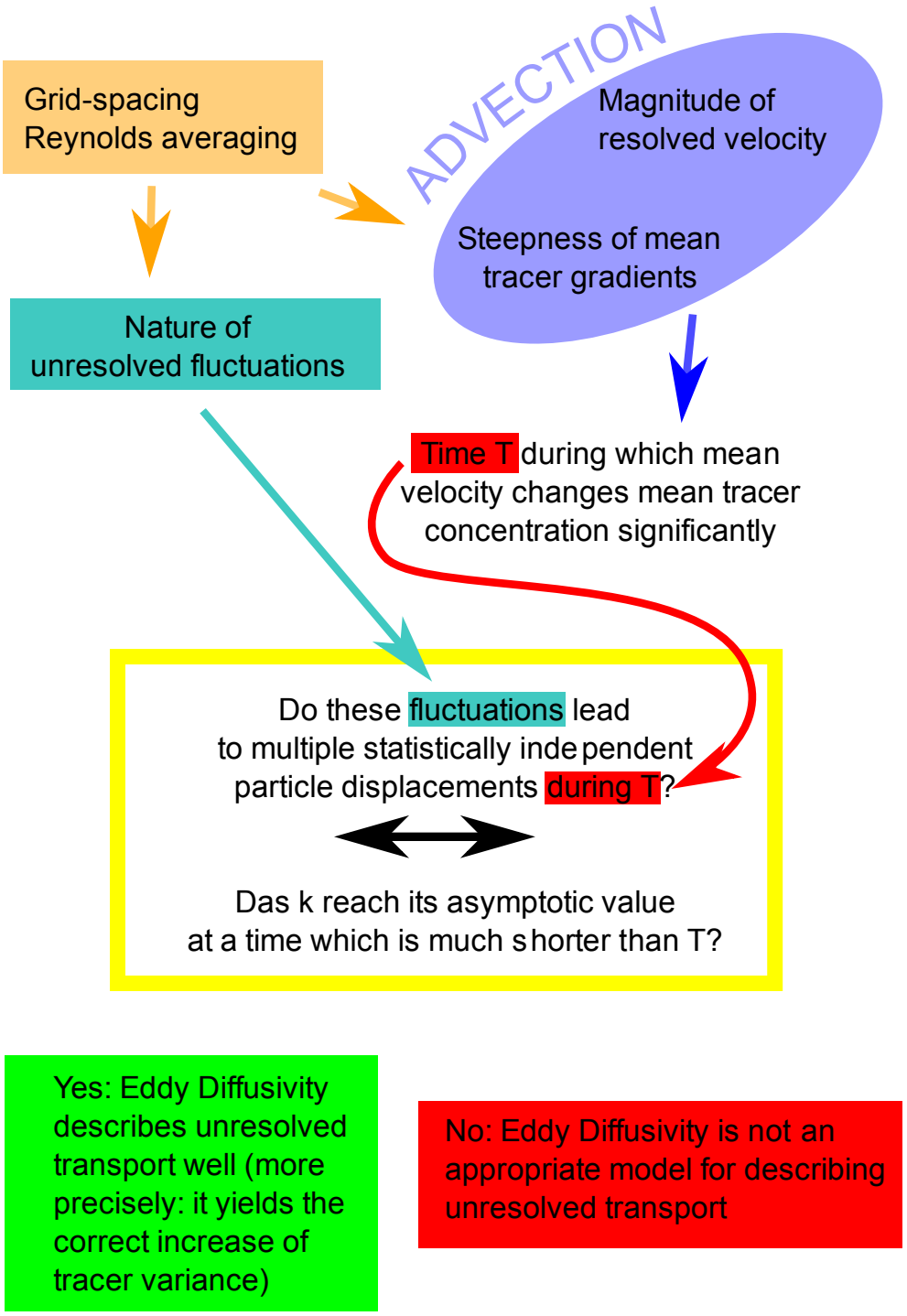

Figure 2: The grid-spacing of an ocean component in a numerical climate-model determines the resolution of the model-velocity. This velocity field is a Reynolds-averaged field, where the average is a time- or space-average. The resolved velocity has a certain magnitude which advects the tracer. Depending on the steepness of the tracer's gradient, the mean-velocity will induce changes of mean-concentration at a point by means of advective transport. The intervall T during which the concentration is changed significantly by advection, depends therefore on the mean-velocity field and the mean-tracer's gradient. A flux-gradient parameterization of unresolved turbulent tracer transport will only make sense if the nature of the fluctuations is such that it causes multiple, statistically independent sequential particle displacements during the intervall T.

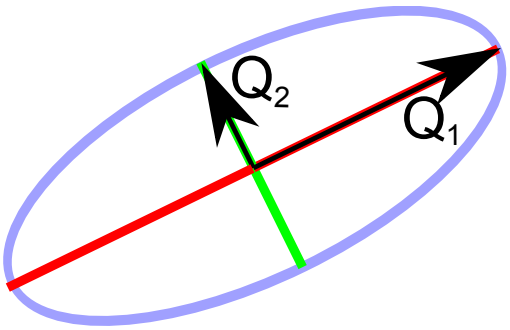

Figure 3: The vectors $Q_1 = \kappa^{sym}_{maj} \cdot \mathbf{E_1}$ and $Q_2 = \kappa^{sym}_{min} \cdot \mathbf{E_2}$ span an ellipse.

1.4 Anisotropy

Previous studies (Rhines & Schopp, 1996) indicate that the diffusivity estimated from eddy-permitting ocean models is characterized by a dominant zonal component. This means that the growth of a tracer patch induced by turbulent velocity fluctuations is faster in zonal than in meridional direction, which is referred to as *anisotropic* turbulent transport. The growth of variance by diffusive processes in two dimensions is described by a diffusion tensor. In this section we introduce the two-dimensional diffusion equation and explain how anisotropic diffusive transport can be expressed mathematically.

Let the three degrees of freedom of a two-dimensional, positive definite symmetric scalar matrix κ^{sym} be denoted by σ_x, σ_y, ρ. Choose the degrees of freedom such that the matrix can be written as

$$\kappa^{sym} = \begin{pmatrix} \sigma_x^2 & \rho\sigma_x\sigma_y \\ \rho\sigma_y\sigma_x & \sigma_y^2 \end{pmatrix}. \tag{51}$$

Then the initial value problem

$$\frac{\partial C}{\partial t} = -\nabla \cdot \kappa^{sym} \nabla C, \qquad -\infty < x < \infty, -\infty < y < \infty \qquad 0 < t < \infty \tag{52}$$

$$C(x, y, 0) = \delta(x, y) \tag{53}$$

has the solution

$$C = \frac{1}{2\pi\sigma_x\sigma_y\sqrt{t\,(1-\rho^2)}} \exp\left(-\frac{1}{2t(1-\rho^2)}\left(\frac{x^2}{\sigma_x^2} + \frac{y^2}{\sigma_y^2} - \frac{2\rho xy}{(\sigma_x\sigma_y)}\right)\right). \tag{54}$$

The shape C is Gaussian at every instant. The matrix κ^{sym} can be decomposed in its principal components:

$$\kappa^{sym} = E \begin{pmatrix} \kappa^{sym}_{maj} & 0 \\ 0 & \kappa^{sym}_{min} \end{pmatrix} E^T, \tag{55}$$

where E is a matrix whose first column is the normalized Eigenvector corresponding to the Eigenvalue κ^{sym}_{maj} and whose second column is the normalized Eigenvector corresponding to the Eigenvalue κ^{sym}_{min}. κ^{sym} is positive definite and so both Eigenvalues are positive. We call the diffusive process modeled by Eq. (53) *anisotropic*, if $\kappa^{sym}_{maj} \neq \kappa^{sym}_{min}$.

In two spatial dimensions, Eq. (23) is written as

$$\frac{\partial C}{\partial t} + \overline{u}\frac{\partial C}{\partial x} + \overline{v}\frac{\partial C}{\partial y} = -\nabla \cdot \begin{pmatrix} \overline{u'C'} \\ \overline{v'C'} \end{pmatrix}. \tag{56}$$

Introducing mixing length scales, we can write

$$\begin{pmatrix} \overline{u'C'} \\ \overline{v'C'} \end{pmatrix} = -\kappa \nabla C \qquad \text{with} \qquad \kappa = \begin{pmatrix} \overline{u'X'} & \overline{u'Y'} \\ \overline{v'X'} & \overline{v'Y'} \end{pmatrix}. \tag{57}$$

The components of κ are

$$\kappa_{ij} = \overline{u_i'(x_0, t_0) \int_{-\infty}^{t_0} u_{jl}'(t)\, dt}. \tag{58}$$

The matrix κ can be split into a symmetric part (κ^{sym}) and an antisymmetric part ($\kappa^{antisym}$):

$$\kappa = \kappa^{sym} + \kappa^{antisym} \qquad \text{where} \qquad \kappa^{sym} = \frac{1}{2}\left(\kappa + \kappa^T\right), \quad \kappa^{antisym} = \frac{1}{2}\left(\kappa - \kappa^T\right) \tag{59}$$

It can be shown (Davis, 1991) that only κ^{sym} leads to a growth of variance, and it is this part that appears in the two dimensional diffusion equation. A discussion of how $\kappa^{antisym}$ can be physically interpreted is beyond the scope of this work.

1.5 Inferring Eddy Diffusivities from Oceanic Drifters: Strategy and Caveats.

- **Random-deployment statistics vs. random-encounter statistics.** In a quasi-stationary flow, single particle statistics at a point **x** can be calculated by repeatedly releasing the same particle at the point between time-intervals of random length. Since the statistics of the flow do not evolve, each individual deployment time can be viewed as being the start of an individual experiment, i.e. each deployment time can be interpreted as time 0 after release. The method of continuously releasing particles at random times into a flow is called *random-deployment* (Davis, 1991). Alternatively, one or more particles can be released at a single instant. The times at which any particle passes the point **x** can again be viewed as being the start of an individual experiment. If a nondivergent flow is sampled with particles, then random-encounter statistics and random-deployment statistics are equal, provided that the density of particles is uniform within the flow (Davis, 1991).

- **Ensemble-averaging vs. spatial averaging over a finite area.** The Lagrangian statistics in the previous sections are obtained by ensemble-averaging particles which depart from the same point, or , in a quasi-stationary flow, particles which occupy the same location at different times . Such techniques are impractical for sampling the ocean. Floats in the ocean are usually released at a certain location and then drift in the ocean for years; They are not recollected and set out on the same point again. It is therefore impossible to obtain random-deployment averages from most of the available observational data. Furthermore, floats in the ocean never occupy the exact same location at any point in time. Random-encounter statistics can therefore not be obtained from observational data. A simple solution is to partition the domain into small regions Ω_i and calculate spatial averages within these regions. The region over which the average is taken, is then interpreted as a 'point' of finite extent. The method of random-encounter statistics at a point can be extended to a region of spatial averaging; Instead of averaging over floats which occupy the exact same point, the average is taken over floats which are located anywhere within the region. We will call this type of average *FARE-average* (finite-area random-encounter average). It might be expected that spatial averaging introduces problems when the Eulerian mean properties of the flow vary within the region of averaging. This issue will be discussed below.

- **Eulerian mean velocity vs. Lagrangian mean velocity.** Differences between the mean velocity of particles and the Eulerian mean velocity can be caused by:

- Stokes drift
- Diffusion bias: Assume that κ is spatially variant. Drifters which are released at a single point will generate a mean particle motion towards regions of high κ. A point release of drifters is an example of a highly nonuniform distribution of drifters. In the case of uniform distribution, all fluid particles are represented by drifters and there is no diffusion bias.
- Array bias: If the ensemble mean concentration within an area of averaging is nonuniform, then an Lagrangian estimate of the space-averaged Eulerian velocity may be biased. As in the case of diffusion bias, a uniform distribution of drifters leads to statistics that are unaffected by array bias.

If the Stokes drift is zero, the Lagrangian mean particle velocity of particles with nonuniform distribution can be interpreted as a concentration-weighted area average of the Eulerian velocity $\mathbf{U}$ plus a diffusion bias proportional to the spatial gradient of κ. The difference between Lagrangian mean velocity and Eulerian velocity, which is caused by Stokes drift, arises wether or not the particle distribution is uniform. We will address this issue briefly and compoare the Eulerian mean velocity calculated by time-averaging the 5.5 year model data and estimate of Eulerian mean velocity by means of Lagrangian sampling. Furthermore, we calculate the Lagrangian mean particle velocity.

- **Horizontally sheared mean flow and spatial averaging.** It was mentioned above that spatial averaging introduces difficulties when the mean properties of the flow vary within the region of averaging. To illustrate the problem, consider a quasi-stationary flow with a horizontally sheared Eulerian mean. Assume that, due to the shear, the Eulerian mean velocity varies substantially within a certain averaging region Ω_m. The FARE-average for Ω_m is a constant within Ω_m, and does not contain information about the sheared Eulerian-mean flow. Since fluctuations u' for an individual float are computed by subtracting an average from the instantaneous velocity, the fluctuation computed from the FARE-average will be different to the one computed from the Eulerian mean field.

  If fluctuations u' computed from the FARE-average are biased by mean shear, then κ_{sym} in (59) is also biased by the mean shear. κ_{sym} is in this case not completely determined by the growth rate of variance caused by random fluctuations, but it is modified by a mean property.

- **Isobaric vs. nonisobaric floats.** The pressure along trajectories of oceanic floats is approximately constant. Consequently, isobaric subsurface floats do not accurately follow vertical flow and this causes floats to disperse differently from particles and to be differently advected by generalized Stokes Drifts (Davis, 1991).

- **Lateral vs. horizontal transport** While it is critical to separate vertical and diapycnal transport, lateral and horizontal transport can generally be interchanged (Davis, 1991).

- **Quasi-stationarity** The theory developed so far is founded upon the conjecture that the general circulation is quasi-steady. However, few information is available on the variability of the ocean circulation on low frequencies.

2 Method

We calculate Lagrangian single-particle statistics from the velocity field of an eddy-permitting model of the North Atlantic and aim to extract information that is relevant to eddy-diffusivity parameterizations for turbulent dispersion.

We use two distinct methods to infer timeseries of κ. In the first experiment (EXP1), we adopt the computational techniques of Swenson & Niiler (1996) to compute particle statistics. Swenson & Niiler (1996) analyze observational data from surface drifters in the California Current. Their method is based on the work of Davis (1991). The region of interest is partitioned into subdomains in which statistics are computed by spatial averaging, as outlined in Section 1.5. In particular, the velocity fluctuations of an individual particle u' in (47) are computed with respect to a spatial average.

We compare the results obtained in EXP1 with an experiment (EXP2) in which the velocity fluctuations u' are computed with respect to the high resolution Eulerian time-mean field. In this case there is no spatial averaging involved in obtaining u'. It was mentioned above that spatial averaging (used in EXP1) introduces difficulties when the mean properties of the flow vary within the region of averaging. Oh *et al.* (2000) perform a numerical simulation of idealized turbulent particle motion to show that estimates of diffusivity based on the minor principal component are, in contrast to other estimates, insensitive to ensemble averaging over particles taken from a finite area in a shear mean flow. In their numerical experiment, the two-dimensional turbulent velocity field is a homogeneous and stationary random field. The random particle motion is a stochastic process characterized by an exponential particle velocity autocorrelation. The diffusivity can be determined from the parameters of the stochastic model and is therefore known a priori. Oh *et al.* (2000) compare different Lagrangian sampling methods and compare their sensitivity to shear of the mean flow. They conclude that ensemble averaging over particles taken from a finite area in a shear mean flow leads to an anisotropic diffusion tensor, and demonstrate that the minor principal component converges towards the a priori known value of diffusivity. The question arises whether this result applies not only to the idealized turbulent field in the work of Oh *et al.* (2000), but also to turbulence in the real ocean.

Oh *et al.* (2000) analyze drifters in the East Sea, drogued at 15m depth. They compute the time-evolution of the diffusivity tensor's principle components with various averaging techniques and note that the minor principle compenent attains in most cases an asymptotic value within the first 40 days, while the major principle component does not converge. Based on the hypothesis that this phenomena is caused by the shear of the mean flow, as in their theoretical study, they conclude that the best chance to obtain reliable estimates of diffusivity is from the time-series of the minor principal component. Lagrangian data from a realistic ocean model can provide a test for this hypothesis (Kamenkovich *et al.*, 2009). In principle, the bias resulting from the mean shear can be determined in the model, since the Eulerian mean velocity field is known. After correction of the bias, the two principle components should have either the same value in case of isotropic diffusion, or a different value indicating anisotropic diffusion. We therefore try to correct the bias by the mean shear in EXP2 by including the Eulerian mean velocity field in the analysis.

The model. We use a mesoscale-eddy-permitting model of the North Atlantic Ocean with horizontal resolution of $1/12^o \cos(\phi) \times 1/12^o$ (where ϕ denotes latitude) ranging from about 10 km at the equator to about 5 km in high latitudes. The model domain extends from 20^o S to 70^o N with open boundaries at the northern and southern boundaries, with a restoring zone in the eastern Mediterranean Sea and with climatological surface forcing (Barnier *et al.*, 1995). There are 45 vertical geopotential levels with increasing thickness with depth, ranging from 10m at the surface to 250m near the maximal depth of 5500m. The model is based on a rewritten version2 of MOM2 (Pacanowski, 1995) and is described in detail in Eden & Greatbatch (2008).

Initial particle distribution. The initial position of every particle is contained within a box spanning the width of the Atlantic Ocean in zonal direction and ranging from $-20°$S to $65°$N in meridional direction, with a depth of ranging from 100m to 6000m. Initially, particles are distributed within this box with a constant spacing of about $1.8°$ in latitudinal and longitudinal direction. This corresponds to a distance between two neighboring floats of about 200km in latitudinal direction. In zonal direction the distance ranges from 85km in high latitudes to 200km in low latitudes. The

spacing in the vertical direction is 125m throughout the water column. Floats are initially distributed in depths ranging from 100m to 6000m. The array contains land, and the number of wet floats is about 50000.

Particle trajectories. Floats are assumed to be of zero mass, neutrally buoyant and move with the local three dimensional flow during each time step (Pacanowski, 1995). For the numerical integration, the simple Euler forward timestepping scheme is modified to take account of convergence of meridians. The Eulerian velocity field is integrated with a timestep of 5 min. Snapshots of the Eulerian velocity field are available in intervals of 3 days and are linearly interpolated with an interpolation interval of 2 hours. We integrate the particles for 2 hours, during which the Eulerian velocity field is time-independent. After two hours we update the Eulerian velocity field to the interpolated value and continue the integration. For further analysis we write down the position of the floats every 3 days. This results in about $3 \cdot 50000$ timeseries for zonal, meridional and vertical position that span 5.5 years with a temporal resolution of 3 days. For each float we also write down the Eulerian velocity at each position. In this respect the extracted data differs from real float data, in which the Eulerian field is unknown and the velocity at each position has to be calculated with finite differences from the particle positions and the time interval between the positions.

Pseudo-trajectories. Multiple pseudo-trajectories are formed from a single individual 5.5-year trajectory by dividing it into several subsections. After 60 days of integration, a floats (let's call it float A) position is marked. The mark corresponds to the end-point of a pseudo-trajectory (pseudo-float B1). After another 60 days of integration, float A's position is marked again and this mark corresponds to the end-point of the next pseudo-trajectory B2. The number of wet pseudo-trajectories amounts to about 1.5 million.

Binsize. The particle statistics are mapped to a grid with dimensions of 30 points in longitudinal direction, 74 points in the zonal, and 19 points in the vertical direction. Gridbox dimensions span 1.2° in meridional direction and 2.8° in zonal direction. This corresponds to a meridional edge length of about 130km and a zonal edge length of 200km (high latitudes) to 315km (low latitudes) for each gridbox. The extent in vertical direction is 300m.

Efficient sampling. For each gridbox, we aim to obtain a set of pseudo-trajectories with statistically independent floats, i.e. floats that do not exhibit similar motions due to spatial or temporal proximity in the Eulerian velocity field. We assume that the gridbox size is equal or larger than the decorrelation length. If we assume that one statistically independent float is observed per month and per bin, then it is desireable to observe about 70 floats in a single bin during the 5.5 years of integration. This estimate depends on the decorrelation length and decorrelation time of the flow and can vary strongly within the domain.

Mapping of Lagrangian statistics to Eulerian data. Every gridbox is associated with a set of pseudo-trajectories. A pseudo-trajectory is part of this set if its endpoint is located within the gridbox. Lagrangian statistics that are mapped to a grid box are computed from this set of pseudo-trajectories.

Experiment 1 (EXP1).

- *Eulerian mean velocity.* The estimate for the Eulerian mean velocity is estimated by averaging the particles' velocity at their endpoints.

- *Eulerian velocity fluctuation.* The estimate for the velocity fluctuation $u'(x_0, t_0)$ in Eq. (47) is calculated by subtracting the particle's velocity at its endpoint from the estimate for Eulerian mean velocity.

- *Mean displacement.* For each position within a pseudo-trajectory, the distance between the position and the end-point is calculated. This yields a timeseries of distances, or displacements, for each pseudo-trajectory. The distance equals 0 at the endpoint. The mean displacement is the time series of average distances, whereby the average is calculated over the

pseudo-trajectories that are contained in the gridbox set. We cut off the time-series of mean displacement at the time when either the zonal component of mean displacement exceeds half of the gridbox width in zonal direction or the analogous event happens in the meridional or vertical direction.

- *Displacement perturbation.* For each pseudo-trajectory, the time-series of displacement perturbation is computed by subtracting the time-series of mean displacement from the time-series of displacement.

- *Diffusion tensor.* The covariance between velocity perturbation and displacement perturbation is calculated, yielding a time-series of tensors with four components.

Experiment 2 (EXP2).

- *Eulerian mean velocity.* The Eulerian mean velocity is calculated by time-averaging the 5.5 year Eulerian velocity with high spatial resolution.

- *Mean displacement.* The mean displacement for each pseudo-trajectory is calculated by backward-integrating the time-averaged 5.5 year Eulerian mean velocity from the endpoint of each trajectory. We cut off the timeseries for the mean flow at the same points as in EXP1.

The other manipulations are the same as in EXP1.

Error bars. We outline the variant of the bootstrapping method which was used to obtain the errorbars in Fig. 5-7. The bootstrapping method is described in Efron (1979). We construct 50 resamples of the observed dataset (the pseudo-trajectories) in every bin, each of which is obtained by random sampling with replacement from the original dataset. The resamples contain the same number of pseudo-trajectories as the original dataset. Timeseries for κ^{sym} are computed from each of the 50 resamples, and we compute error bars by calculating the standard deviation of the 50 data-points at each time lag.

What must be considered before interpreting the results.

- **Array bias and diffusion bias.** In our numerical integration, particles are distributed with a constant spacing 200km along the zonal direction. The spacing in the meridional and vertical directions are 200km and 300m. The particle density is therefore initially lower in low latitudes. The domain is not closed and no drifters are seeded into the water entering from the boundaries. On the other hand, water exiting the domain contains drifters and this leads to a loss of about 50000 floats during the 5.5 year simulation, which corresponds to about 3 percent of the total number of inital wet pseudo-particles. We have not been able to quantify a possible bias arising from the non-uniform initial particle distribution and the non-uniformity caused by particle loss, but we believe that the variations of density within a grid cell are too small to affect the results significantly.

- We assume that the statistics of the flow field produced by the numerical model are stationary.

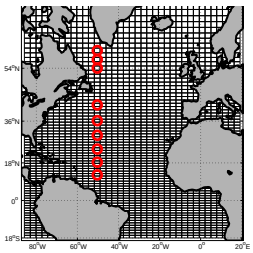

Figure 4: 9 Stations at $50, 32^o$ West. Latitudes are: 12.39^o N, 18.33^o N, 24.28^o N, 30.23^o N, 36.18^o N, 42.12^o N, 54.02^o N, 56.4^o N, 58.78^o N,

3 Results

In this section we show the results of our calculations for the transect at 50^o W (Fig. 5 to Fig. 13) and for $z \approx 650m$ (Fig. 14(a) to Fig. 14(d))
In Fig. 5- 10 we plot timeseries of κ_{max}^{sym} and κ_{min}^{sym} for selected latitudes and depths. The coordinates of the stations are plotted in Fig. 4. Fig. 5- 7 show results from EXP1 with a pseudo-trajectory length of 60 days, and we repeat the same calculation with pseudo-trajectorie of 200 days, the results of which are shown in Fig. 8- 10. The computational method we use, forces us to make a compromise between statistical accuracy and information at longer lags. For a given number of independent float trajectories, we can increase the timelag only at the cost of lower statistical significance. This is because the analysis of longer lags requires longer pseudo-trajectories, which results in a lower number of total pseudo-trajectories due to the fixed number of available 5.5-year trajectories. In the calculation with the 200-day pseudo-trajectories, the lower number of pseudo-trajectories results in larger error bars also at lags shorter than 60 days, simply because there are less observations available for each timelag. In this section we discuss how results obtained with 60-day pseudo-trajectories differ from those obtained with 200-day trajectories. However, we only use results from the former calculation for the rest of this work, since we believe that the statistical significance of the results obtained from the latter calculation (200-day pseudo-trajectories) is too low to lead to any conclusions. Although we do this at the cost of having available only a relatively short timelag for analysis, we think that two months can be regarded as a reasonable timespan for the relevance of unresolved tracer transport with relatively steep mean-gradients in a transport equation, especially in regions with strong mean flow (e.g. western boundary currents). Since our analysis aims to be of relevance for parameterizing unresolved transport in ocean-components of climate models, the time-interval for which statistical transport properties are to be analyzed is bounded; If a transport equation consists of an advective part governed by the mean flow, and a flux-gradient parameterization part which is determined by statistical properties of unresolved velocity fluctuations, then the time-lag for which the statistics are observed must be smaller than the typical time during which the mean flow changes the mean tracer field significantly. The typical time during which the mean flow changes the tracer concentration depends not only on the mean velocity but also, and especially in the case of a stationary mean flow, on the steepness of the tracer's gradients.
The figures show that at 650m depth and above, the timeseries of κ_{max}^{sym} and κ_{min}^{sym} ends before 60 days in some gridboxes, because the mean displacement of the floats is not contained whithin the gridbox after that time. The timeseries which represents the mean over the 50 bootstrap results ends at the lag at which the mean displacement of more than 25 resamples exit the grid-box volume. κ_{min}^{sym} and κ_{max}^{sym} overlap at lag zero and after some variable time, the difference between κ_{min}^{sym} and κ_{max}^{sym} becomes significant in almost all the gridboxes until the end of the 60-day lag. However, in the lower left plot of Fig. 5 we see that the eigenvector which initially corresponds to the small eigenvalue ends up to become the eigenvector to the larger eigenvalue. The length of the interval

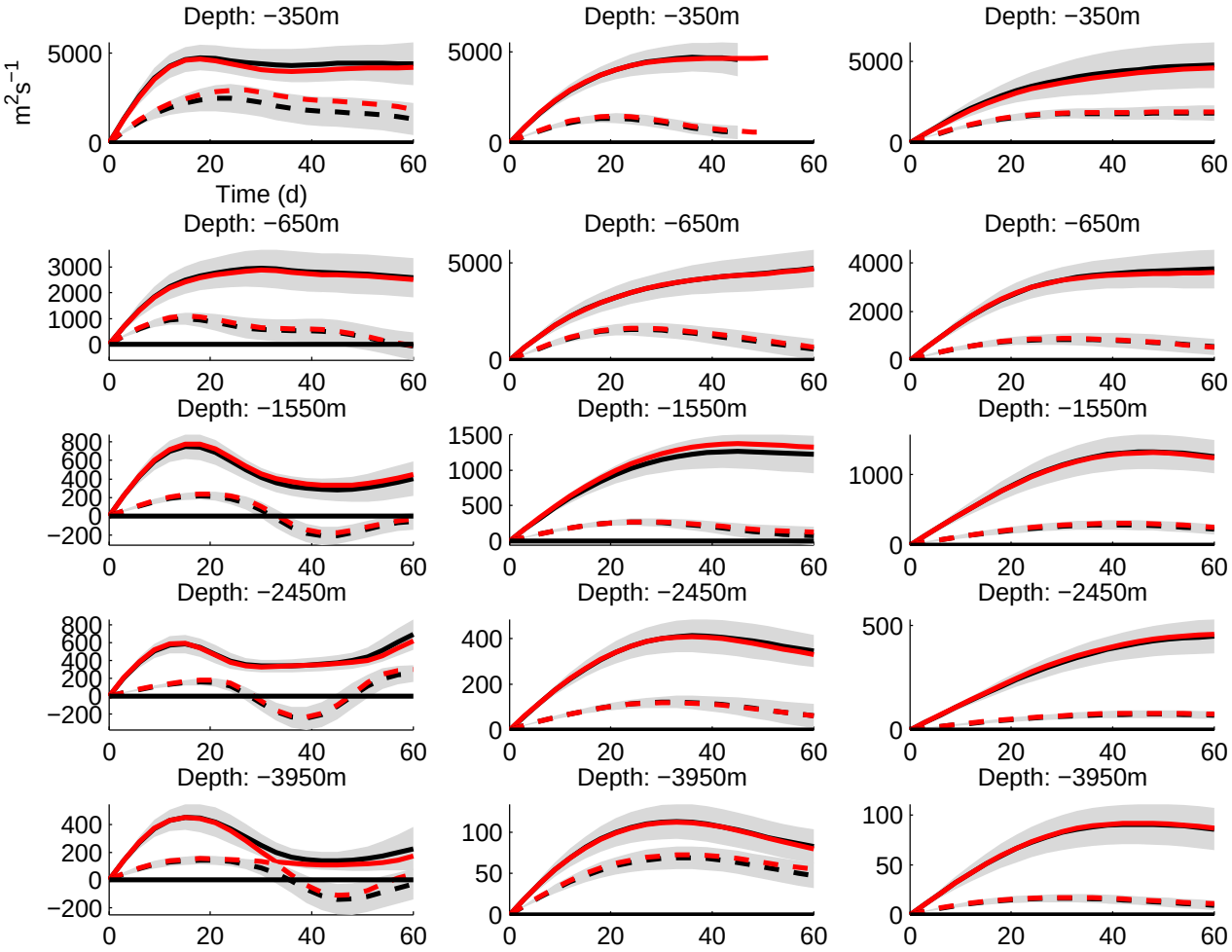

Figure 5: Evolution of κ_{max}^{sym} and κ_{min}^{sym} in time at different latitudes and depths. The left column refers to the southernnmost point in Figure 4, at 12.39^o N. The columns to the right describe the points 18.33^o N and 24.28^o N. Timeseries of κ_{max}^{sym} (κ_{min}^{sym}) for various depths are plotted in solid (dashed) red. Black lines and grey shading are the mean and standard deviation of 50 bootstrap samples.

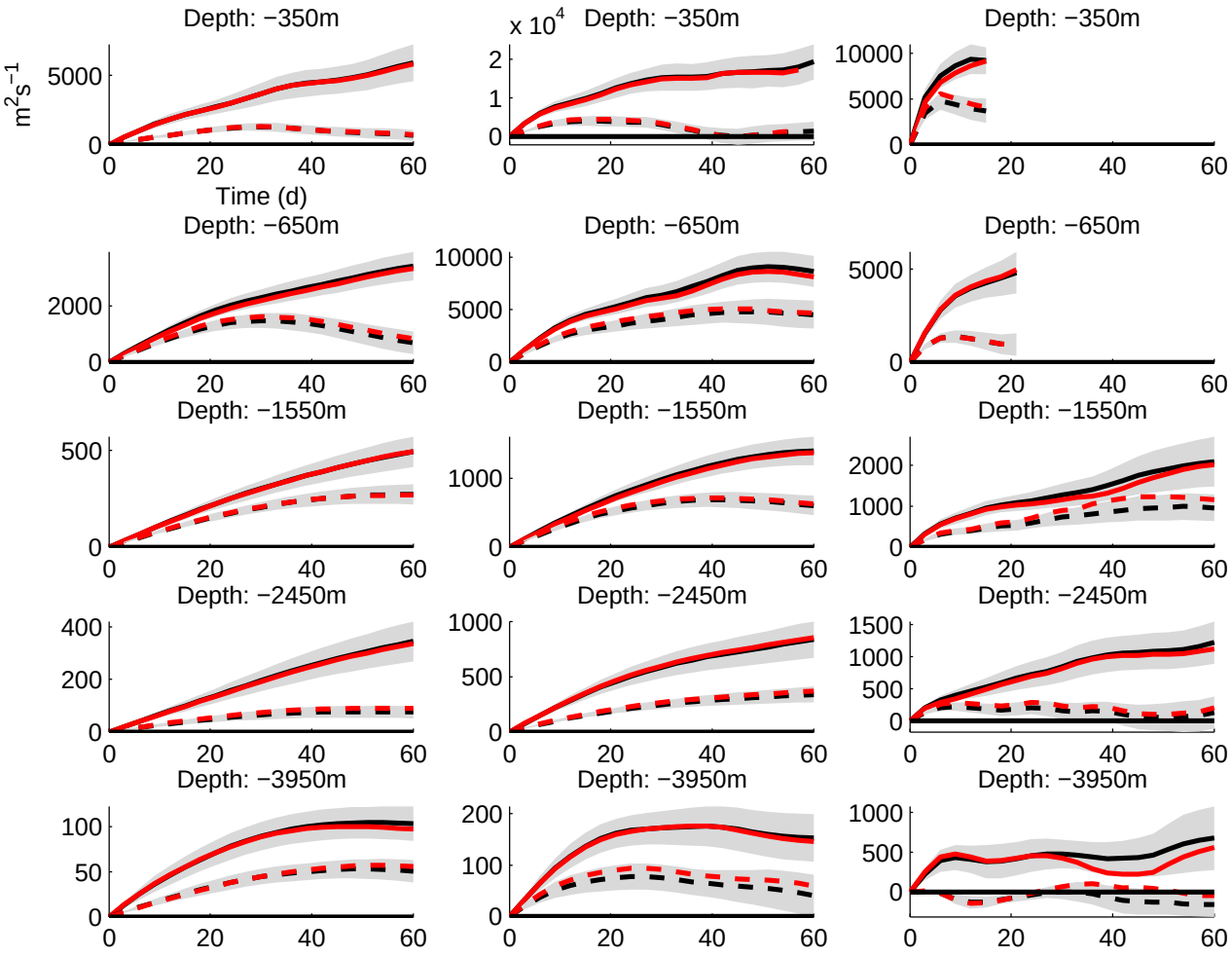

Figure 6: Evolution of κ_{max}^{sym} and κ_{min}^{sym} in time. The left column refers to the fourth point counting from South in Figure 4, the columns to the right describe the points in northward direction. Timeseries of κ_{max}^{sym} (κ_{min}^{sym}) for various depths are plotted in solid (dashed) red. Black lines and grey shading are the mean and standard deviation of 50 bootstrap samples.

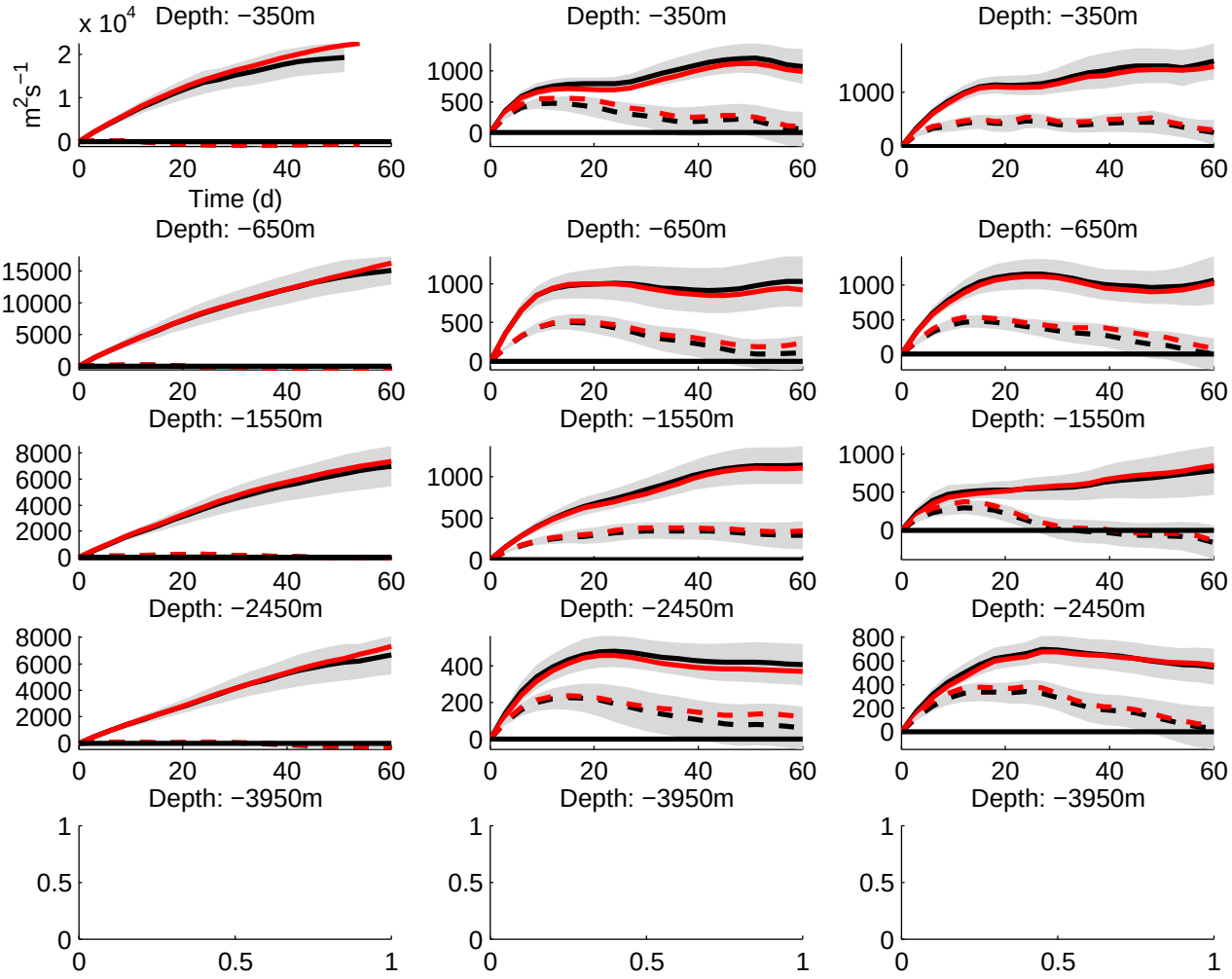

Figure 7: Evolution of κ_{max}^{sym} and κ_{min}^{sym} in time. The left column refers to the third point countint from North in Figure 4, the columns to the right describe the points in northward direction. Timeseries of κ_{max}^{sym} (κ_{min}^{sym}) for various depths are plotted in solid (dashed) red. Black lines and grey shading are the mean and standard deviation of 50 bootstrap samples.

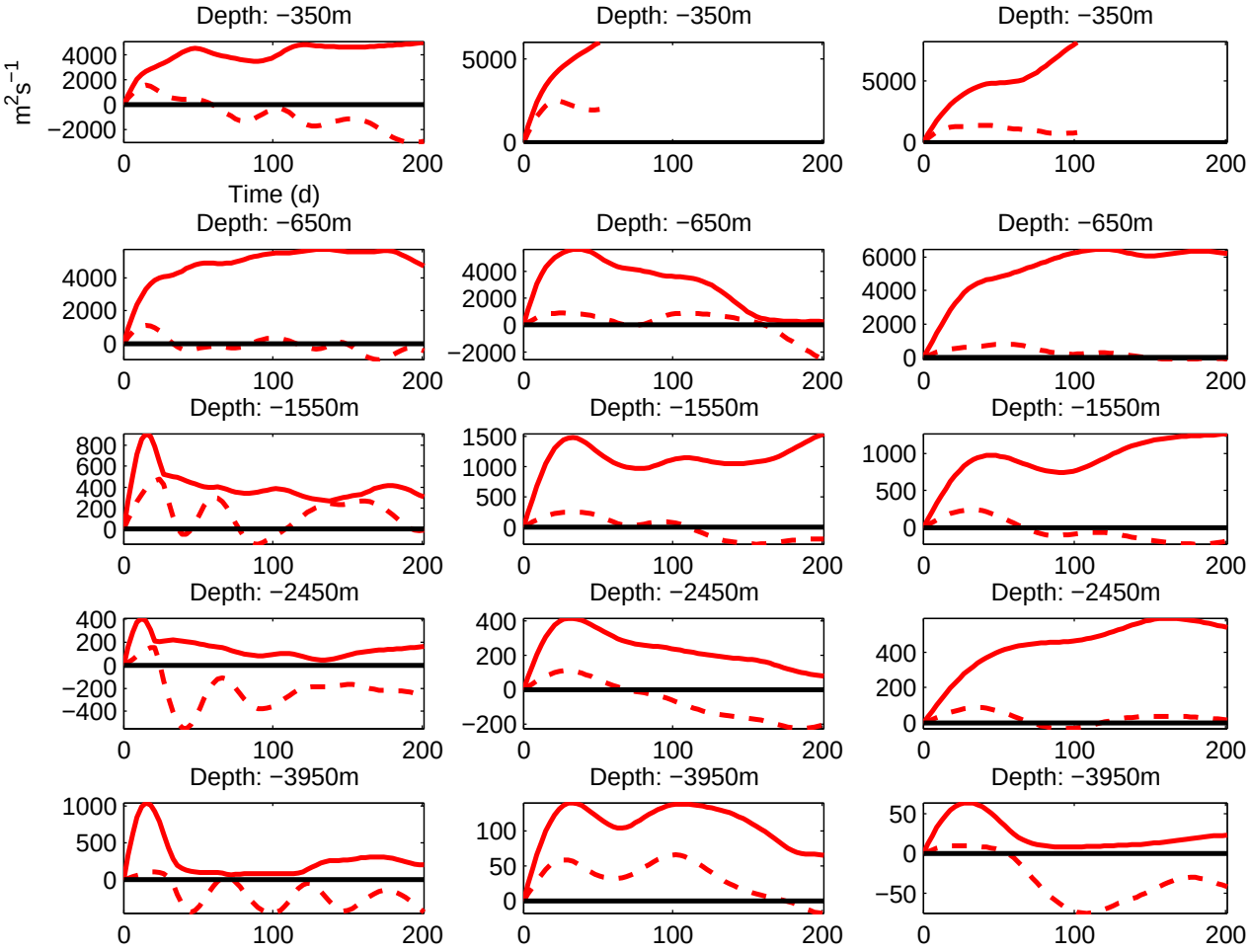

Figure 8: Evolution of κ_{max}^{sym} and κ_{min}^{sym} in time at different latitudes and depths. The left column refers to the southernnmost point in Figure 4, at 12.39^o N. The columns to the right describe the points 18.33^o N and 24.28^o N. Timeseries of κ_{max}^{sym} (κ_{min}^{sym}) for various depths are plotted in solid (dashed) red.

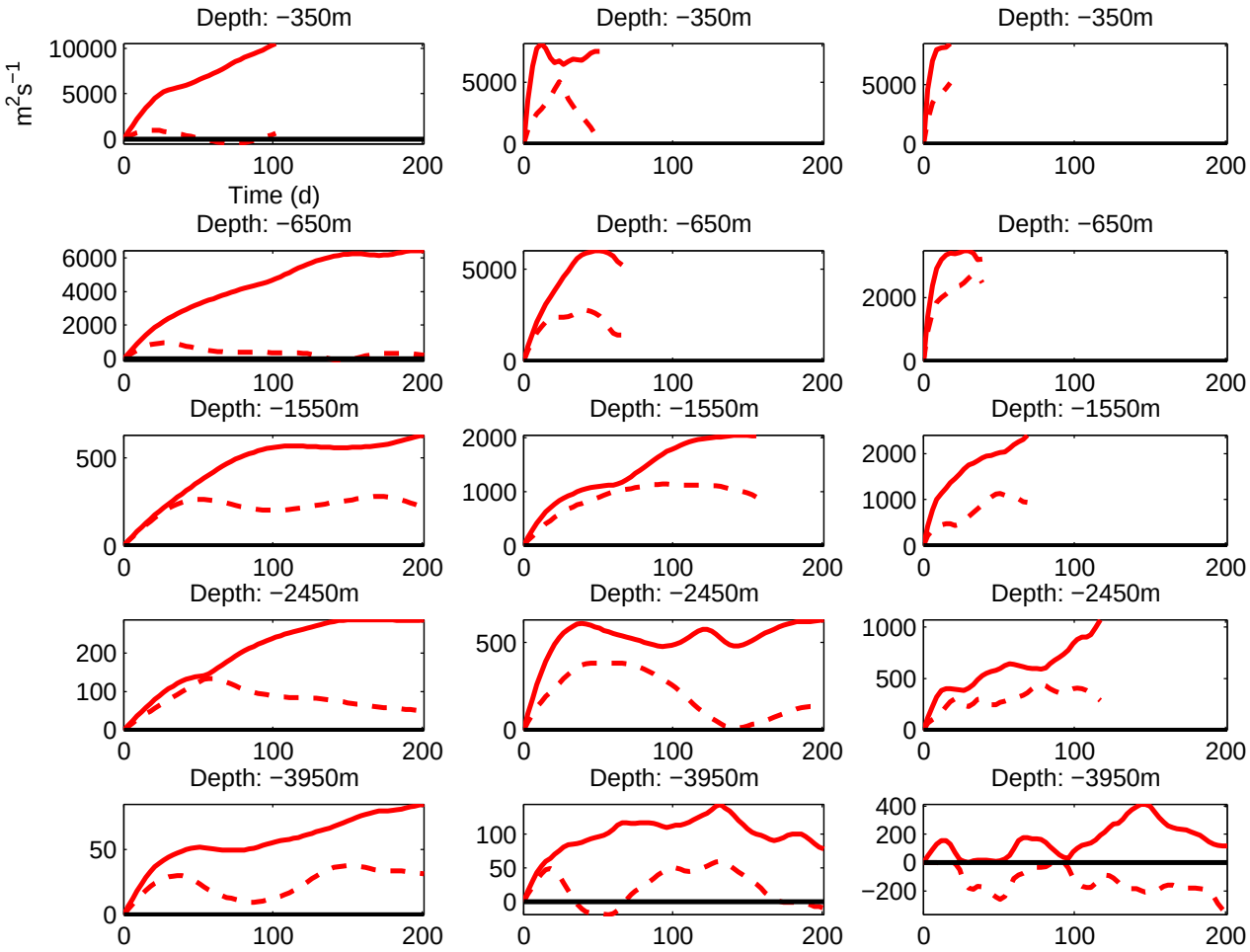

Figure 9: Evolution of κ_{max}^{sym} and κ_{min}^{sym} in time. The left column refers to the fourth point counting from South in Figure 4, the columns to the right describe the points in northward direction. Timeseries of κ_{max}^{sym} (κ_{min}^{sym}) for various depths are plotted in solid (dashed) red.

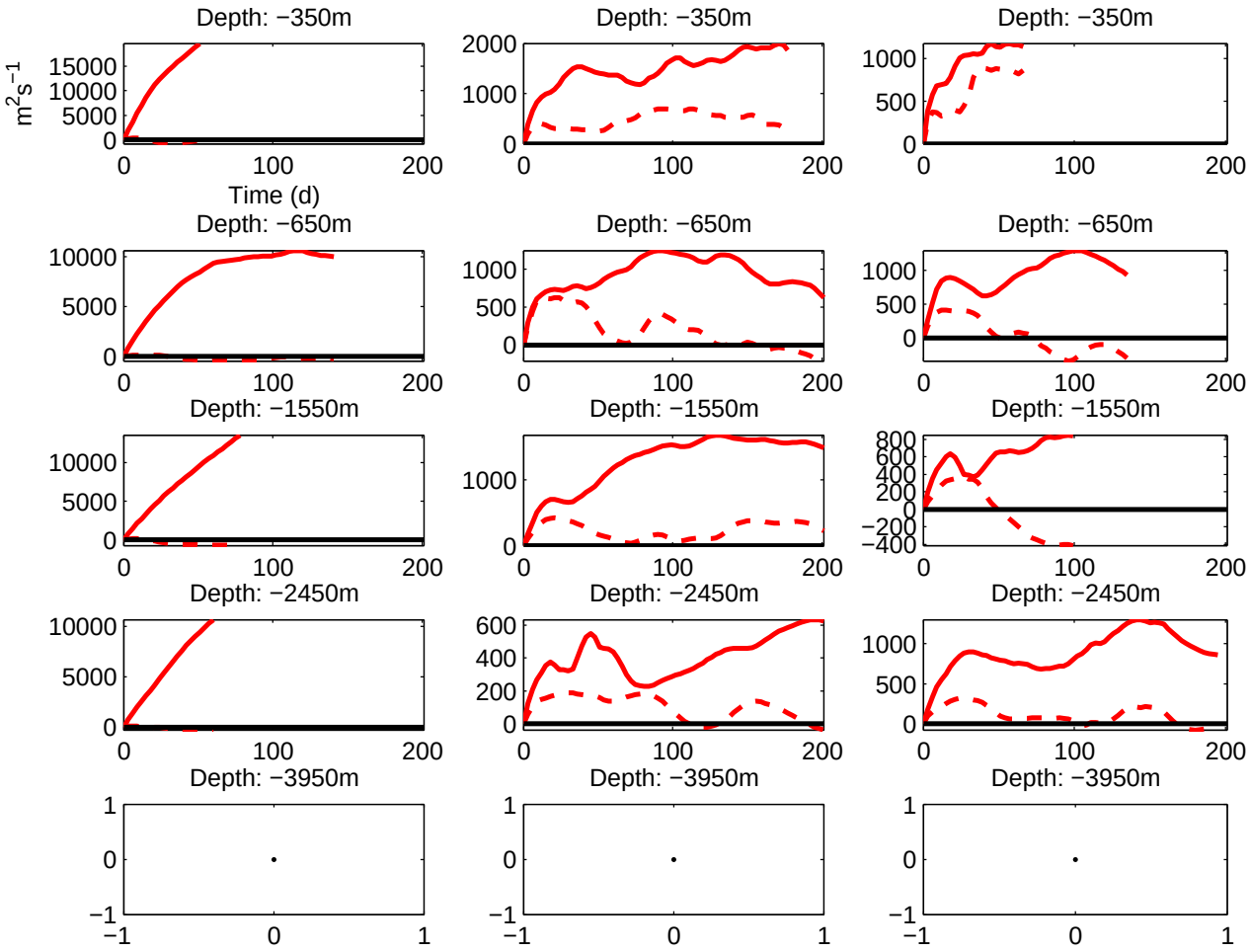

Figure 10: Evolution of κ_{max}^{sym} and κ_{min}^{sym} in time. The left column refers to the third point countint from North in Figure 4, the columns to the right describe the points in northward direction. Time-series of κ_{max}^{sym} (κ_{min}^{sym}) for various depths are plotted in solid (dashed) red.

during which the principal components usually overlap ranges between 1 to 10 days.
The major principal component is significantly different from zero during the entire 60-day lag in all plotted gridboxes. For the minor principal component, this is only the case outside of the tropical and the subpolar regions. At latitudes south of 18.33^o N and north of 54.02^o N, κ_{min}^{sym} reaches a value that is rarely significantly different from zero at the end of the 60-day lag. A value of zero for κ_{min}^{sym} indicates that the variance of a tracer patch does not continue to grow in direction of the eigenvector corresponding to κ_{min}^{sym}. In situations where $\kappa_{min}^{sym} = 0$ and $\kappa_{max}^{sym} > 0$, a released tracer patch increases only in direction of κ_{max}^{sym}. Between 24.28^o N and 42.12^o N, the value of κ_{min}^{sym} is significantly different from zero in almost all plotted gridboxes.
At times before κ_{min}^{sym} attains its maximum, the values of κ_{max}^{sym} in most plotted gridboxes are either larger than κ_{min}^{sym} by a fraction of κ_{max}^{sym}, or several times larger than κ_{min}^{sym}. The same applies to a certain time after $max(\kappa_{min}^{sym})$ is reached. κ_{max}^{sym} exceeds κ_{min}^{sym} by not more than the 10-fold during this time. Of course, κ_{max}^{sym} is orders of magnitude larger than κ_{min}^{sym} in those cases where κ_{min}^{sym} approaches values that are not significantly different from zero, because κ_{max}^{sym} is significantly different from zero in every plotted gridbox.
The value of $max(\kappa_{max}^{sym})$ and $max(\kappa_{min}^{sym})$ generally decreases with depth (see also Fig. 11(a) and Fig. 11(b)). At every latitude except the lowest, there are depths in which κ_{max}^{sym} increases monotonically until the end of the 60-day lag. The data at 54.02^o N is likely to be biased (see discussion below).
In most cases κ_{min}^{sym} is not monotonically increasing during the 60-day lag. Exceptions occur at 24.28^o N, 30.23^o N and 36.18^o N. At the four southernmost stations, the time at which $max(\kappa_{min}^{sym})$ is reached grows in poleward direction for most depths. In the two northernmost stations, κ_{min}^{sym} attains its maximum during the first 20 days in most depths.
Some of these figures suggest that the value of κ_{max}^{sym} at $\tau = 60d$ might be representative for an asymptotic value, because the curves are flat at the end. Other figures show that the slope is still positive for $\tau = 60d$. However, there is no reason to believe that κ_{max}^{sym} has reached a constant value at the end of the 60-day lag, or continues to grow and reach a constant value at later lags. The 60-day lag is too short to reveal a possible oscillation at lower frequencies. The figure provokes the impression that monotonicity of κ_{max}^{sym} is especially prominent in the Subtropics. Low frequency oscillations of κ_{max}^{sym} in the Subtropics could be explained by a longer eddy turnaround time if the flow is in frozen field regime, or by long Eulerian time scales if the flow is in fixed float regime.
A similar consideration is required for cases where κ_{min}^{sym} reaches values which are not significantly different at the end of the 60-day lag. The question arises whether this is also true for times after the 60-day lag. At 12.39^o N, κ_{min}^{sym} oscillates around zero at depths below 1500m, and lower frequency oscillations could occur in other regions. The spatial averaging used in EXP1 causes κ to be biased by small variations of the mean properties of the flow. We try to correct the bias by the mean shear in EXP2 by including the Eulerian mean velocity field in the analysis (EXP2). The timeseries of κ_{max}^{sym} and κ_{min}^{sym} are almost identical in EXP1 and EXP2, with the exception of gridboxes located at 54.02^o N (see discussion below).
Fig. 8 - 10 show the results obtained from 200-day pseudo-trajectories. In some gridboxes, the evolution of κ_{max}^{sym} and κ_{min}^{sym} differs strongly between the 60-day and the 200-day calculation. An example is shown in the upper left corners of 5 and 8. In Fig. 8, κ_{max}^{sym} increases monotonically throughout the first 60-days, which is not the case in 5. In the third row of the left column in Fig. 8 we see that the eigenvector which initially corresponds to the small eigenvalue ends up to become the eigenvector to the larger eigenvalue. This does not seem to be the case in Fig. 5.

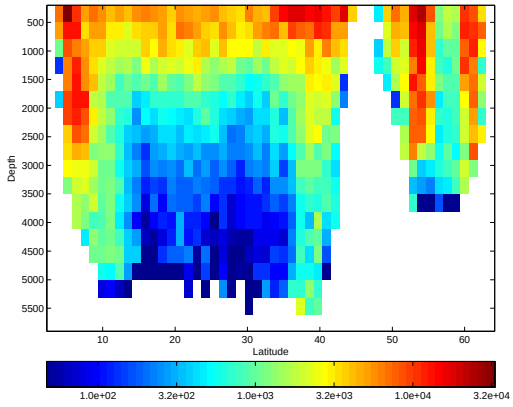

(a) Maximum of κ_{max}^{sym} (m^2/s) over the 60-day lag. Colorbar is logarithmic.

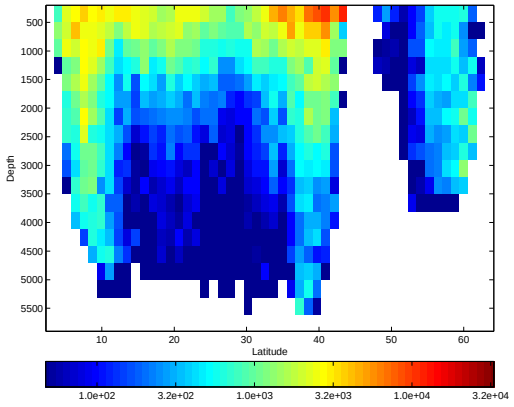

(b) Maximum of κ_{min}^{sym} (m^2/s) over the 60-day lag. Colorbar is logarithmic.

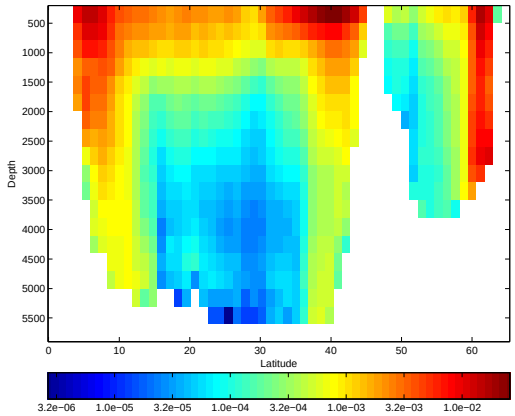

(c) Eddy kinetic energy (EKE) (m^2/s^2) of the Eulerian velocity field, calculated from fluctuations around the 5.5 year mean velocity. Colorbar is logarithmic.

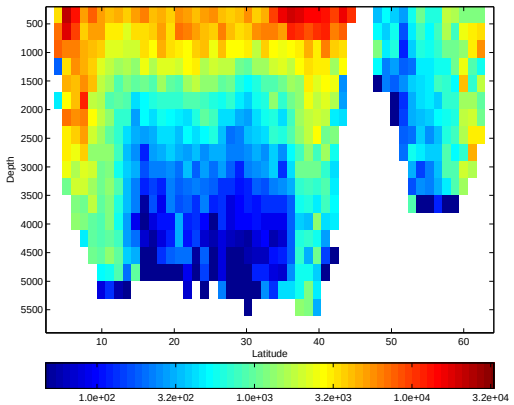

(d) EXP2: Maximum of κ_{max}^{sym} (m^2/s) over the 60-day lag. Colorbar is logarithmic.

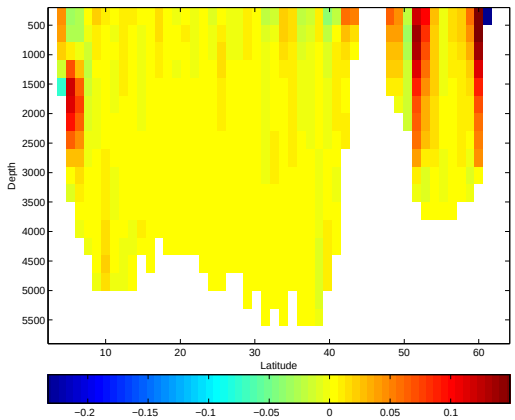

(e) Curl $(1/s)$ of the Eulerian mean horizontal velocity. The high resolution velocity field was averaged within each gridbox. The partial derivatives were computed by finite differencing of the averaged field.

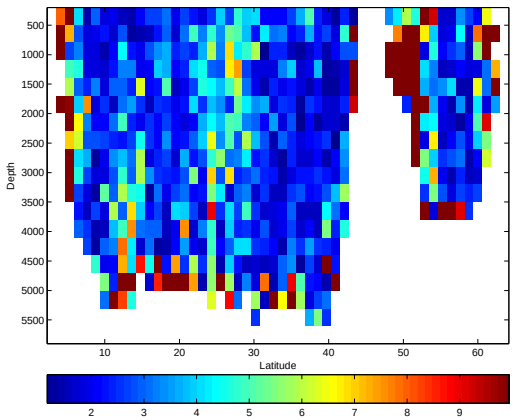

(f) The ratio $max(\kappa_{max}^{sym})/max(\kappa_{min}^{sym})$. The values of κ_{max}^{sym} were taken from EXP2

Figure 11: 50^o W

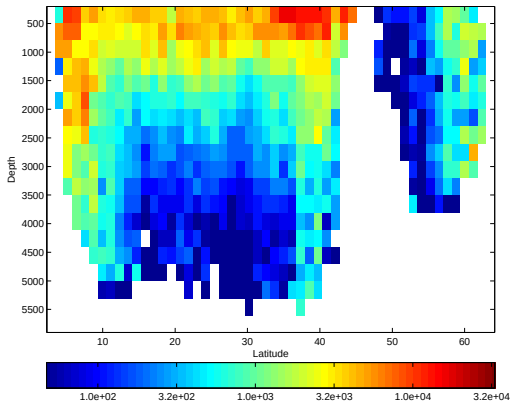

(a) EXP2: $max(\kappa_{xx}^{sym})$ (m^2/s)

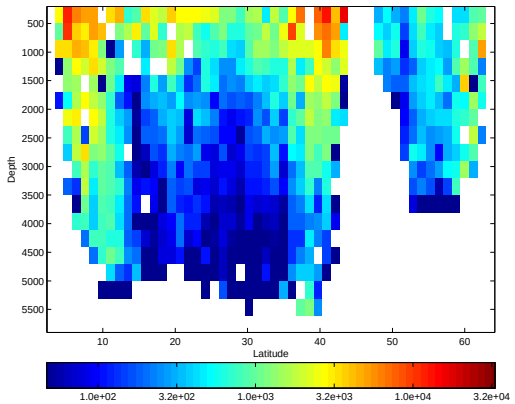

(b) EXP2: $max(\kappa_{xx}^{sym})$ (m^2/s)

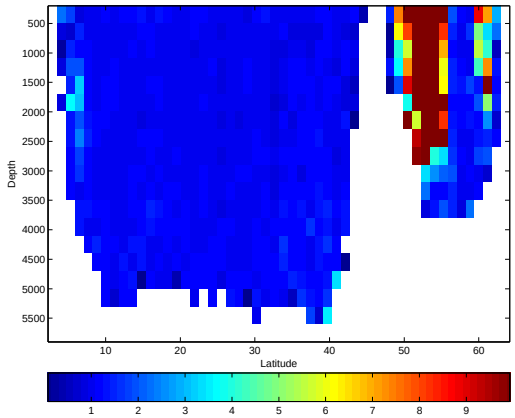

(c) The ratio of $max(\kappa_{max}^{sym})$ calculated in EXP1 to $max(\kappa_{min}^{sym})$ calculated in EXP2.

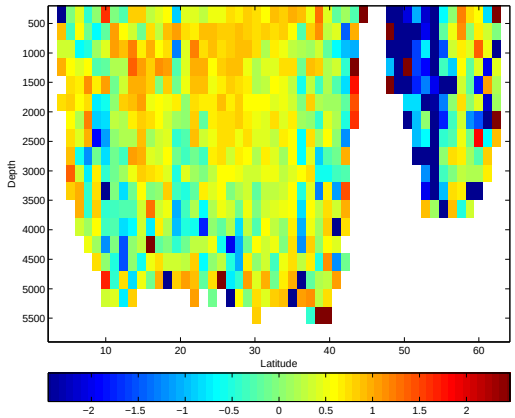

(d) EXP1: $(\kappa_{xx}^{sym} - \kappa_{yy}^{sym})/\kappa_{xx}^{sym}$.

Figure 12: 50^o W

Fig. 11 and 12 show that $max(\kappa_{max}^{sym})$ and $max(\kappa_{min}^{sym})$ are surface intensified and generally decrease with depth. This is also the case for EKE, which is defined as $\frac{1}{2}(\overline{u'^2} + \overline{v'^2})$ where u and v are the Eulerian velocities. Values of $max(\kappa_{max}^{sym})$ range between O(1000) m/s and O(10000) m/s in the gridboxes above 1000m depth, whereas values of $max(\kappa_{min}^{sym})$ range from O(100) to O(10000) m/s in the same depth layers. At 2000m depth, values range from O(100) m/s to 20000 m/s for $max(\kappa_{max}^{sym})$ and O(10) to O(1000) for $max(\kappa_{min}^{sym})$. The spatial structure of $max(\kappa_{max}^{sym})$ and $max(\kappa_{min}^{sym})$ are similar , apart from 50^o N to 55^o N, where $max(\kappa_{max}^{sym})$ exhibits a pronounced local maximum throughout the water column. This feature is not present in the fields of $max(\kappa_{min}^{sym})$ and EKE.
Fig. 11(d) shows $max(\kappa_{max}^{sym})$ from EXP2. We compare the results for $max(\kappa_{max}^{sym})$ calculated with two different methods. In the first method (EXP1), velocity and displacement fluctuations are computed with respect to mean variables that are estimated from Lagrangian data. Oh *et al.* (2000) suggested that this method leads to a sensitivity of the results for $max(\kappa_{max}^{sym})$ to shear mean flow. The second method involves mean variables which are computed from the 5.5 year Eulerian mean velocity field. A comparison of the differences between the results from EXP1 and EXP2, and the curl of the horizontal velocity shows that the differences are associated with large-scale shear mean flow. In Fig. 11(d) there is no local maximum in the region from 50^o N to 55^o N, and the local maxima between 7^o N to 10^o N and between 60^o N to 63^o N are less pronounced. Apart from this

difference, the spatial structure looks similar to the results from EXP1. Fig. 11(e) shows that regions which are characterized by a strong shear in the horizontal Eulerian mean velocity coincide with the regions where EXP1 and EXP2 yield different results for $max(\kappa^{sym}_{max})$. We conclude that horizontal large-scale mean shear causes anisotropy of the diffusivity tensor obtained by FARE-averaging. A comparison between Fig. 11(f) and Fig. 12(c) indicates that large-scale mean shear is not the only cause for anisotropy. In Fig. 11(f) we see that the magnitude of $max(\kappa^{sym}_{max})/max(\kappa^{sym}_{min})$ is of order O(1), with the exception of the region between 48^o N to 51^o N. Higher values are also found at the boundaries, where our method is likely to produce dubious results. Fig. 12(d) indicates that the difference of the zonal and the meridional component of κ^{sym}, scaled by the value of the zonal component. For each gridbox, the data is calculated at the time when κ^{sym}_{max} is maximal. There are regions which are characterized by a higher zonal component, e.g. 25^o N to 35^o N above 3000m Depth. There are also regions with a higher meridional component. Fig. 11(f): The asymptotic limit of $\kappa^{sym}_{max}/\kappa^{sym}_{min}$ is sometimes used as a measure of anisotropy. In our analysis, the asymptotic limit cannot be calculated and we have the choice of comparing the principal components either at the same time-lag or at the same stage of evolution (note that κ^{sym}_{max} and κ^{sym}_{min} reach their maximum at different lags). Fig. 12(d): We compare the magnitudes of κ^{sym}_{xx} and κ^{sym}_{yy} at the time when κ^{sym}_{max} is maximal.

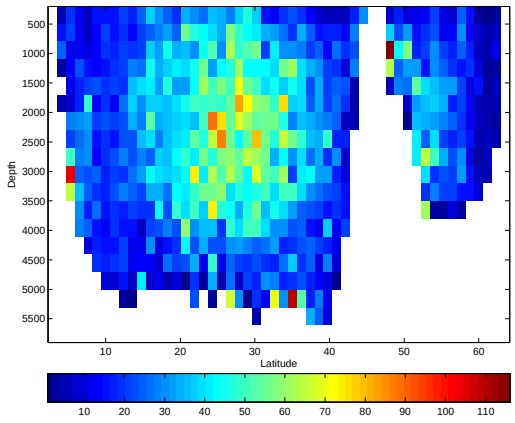

(a) $T_{max} = max(\kappa^{sym}_{max})/EKE$ (days). For $max(\kappa^{sym}_{max})$, the results of EXP2 are used.

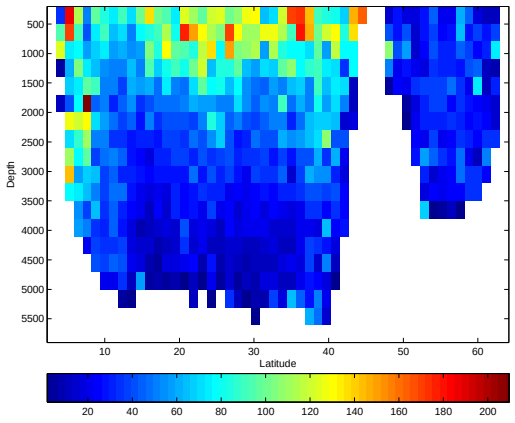

(b) $L_{max} = max(\kappa^{sym}_{max})/\sqrt{EKE}$ (km). For $max(\kappa^{sym}_{max})$, the results of EXP2 are used.

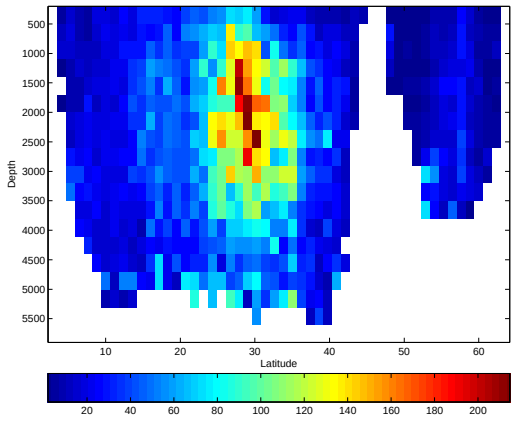

(c) $T^L_{max} = max(\kappa^{sym}_{max})/\frac{1}{2}\left(\overline{u_l'^2} + \overline{v_l'^2}\right)$ (days).

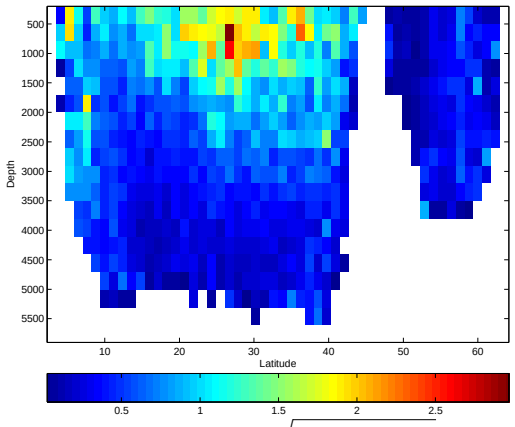

(d) $L^L_{max} = max(\kappa^{sym}_{max})/\sqrt{\frac{1}{2}\left(\overline{u_l'^2} + \overline{v_l'^2}\right)}$ (km).

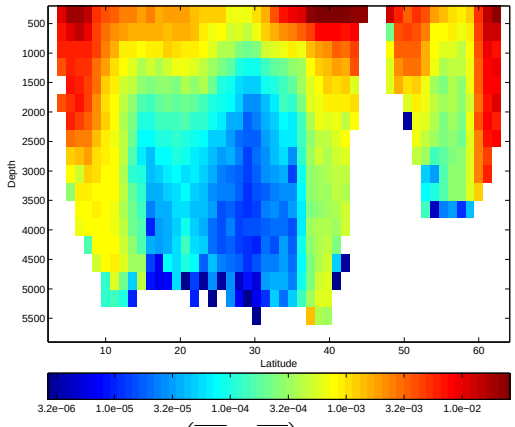

(e) $\frac{1}{2}\left(\overline{u_l'^2} + \overline{v_l'^2}\right)$ (m^2/s^2)

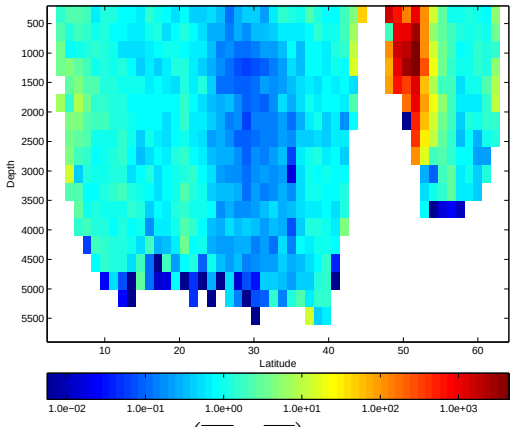

(f) $\frac{1}{2}\left(\overline{u_l'^2} + \overline{v_l'^2}\right)/EKE$

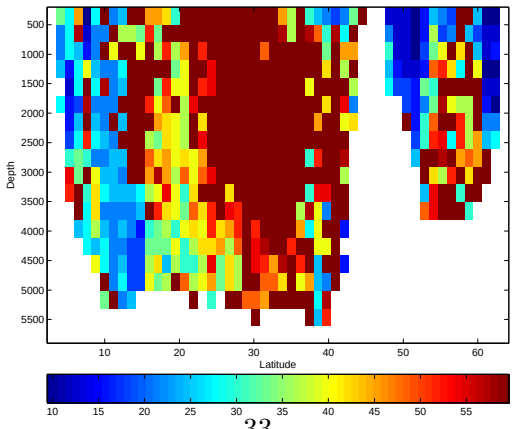

(g) The lag (in days) at which κ^{sym}_{max} is maximal.

Figure 13: 50^o W

Fig. 13(a) shows T_{max}, which is a scalar field in units of time that relates the 5.5 year time-averaged Eulerian velocity field to the maximum of the major principal component during the 60-day lag. T_{max} ranges from 3 to 25 days between 7^o N and 13^o N. In some parts of this region (e.g. at 10^o N), the value of T_{max} does not vary more than 15 days throughout the watercolumn. Between 15^o N and 40^o N, values for T_{max} generally increase with depth until about 2500m depth, and then decrease towards the ocean bottom. Around 28^o N, T_{max} ranges from about 15 to 90 days. In the region between 12^o N and 44^o N, there is a symmetry around 28^o N. Form 47^o N and 64^o N, T_{max} ranges from 2 to 60 days. T_{max} generally decreases to in northward direction. Values of L_{max} are generally surface intensified and decrease with depth in the region south of 45^o N.
For calculation of T^L_{max} we use $\overline{u_l'^2}$ instead of EKE. For calculation of $\overline{u_l'^2}$, we use 120-day trajectories. This is probably not long enough to capture $\overline{u_l'^2}$ in regions which are characterized by a long eddy-turnaround time. This has to be considered when interpreting Fig. 13(f). The spatial pattern of T^L_{max} is similar to that of T_{max}, but not identical. Fig. 13(f) shows that the ratio of $\overline{u_l'^2}$ to EKE is of order O(1) and approximately constant with depth almost everywhere south of the subpolar region. Between 10^o N and 25^o N the ratio is higher than between 25^o N and 35^o N. In the subpolar region, there is a pronounced maximum of $\overline{u_l'^2}/EKE$, with values on the order of O(10^3). The location of the maximum and the region of strong horizontal mean shear largly coincide.
Fig. 13(g): The time at which κ^{sym}_{max} and T_{max} do not have identical spatial distributions.
For the entire region, $max(\kappa^{sym}_{max})$ is neither a linear function of EKE, nor of $\sqrt{EKE}$. However, a linear relationship to EKE in the vertical direction fits better in some latitudes (e.g. 10^o N) than in others (e.g. 28^o N).
In Fig. 14 we show the horizontal structure of some variables. In Fig. 14(a) we see that large values of $max(\kappa^{sym}_{max})$ occur at the Equator, along the western boundaries, at the location where the West Greenland current separates from the continental shelf and west of the Strait of Gibraltar. The pattern is similar to that of EKE (Fig. 14(b)) Fig. 14(c) shows a region of high T^L_{max} in the center of the Subtropical Gyre that spans about 10 degrees in latitudinal direction and almost across the whole width of the ocean basin, excluding the region close to the western boundary. It has values about twice as high than north and south of the region. High values are also found at the equator and south of the equator. Fig. 14(d) suggests that low values are found in the Shadow Zones and above 50^o N.

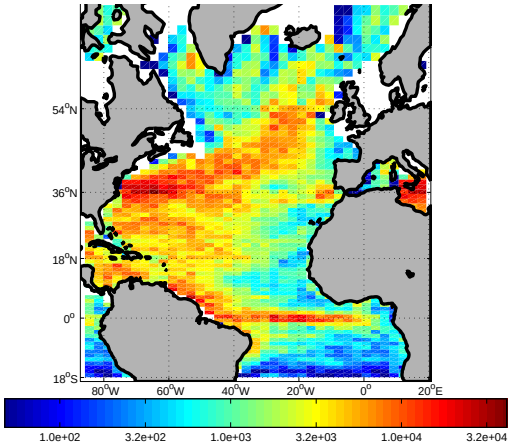

(a) $max(\kappa^{sym}_{max})$ (m^2/s) between 500m and 800m depth.

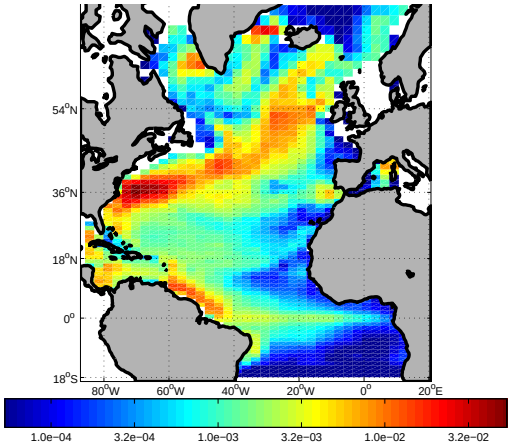

(b) EKE (m^2/s^2) between 500m and 800m depth.

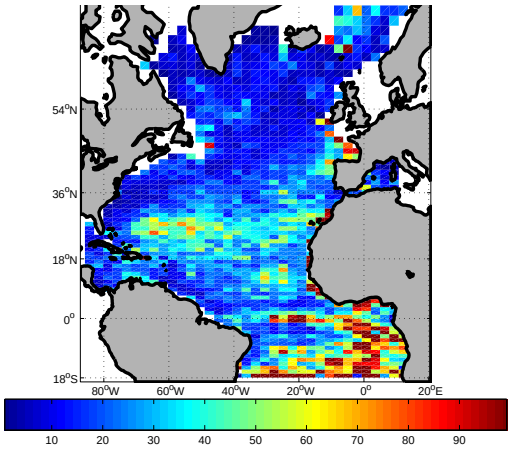

(c) $T^L_{max} = max(\kappa^{sym}_{max})/EKE$ (days) between 500m and 800m depth.

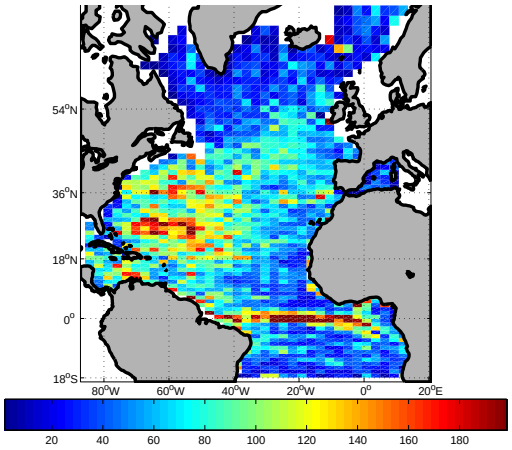

(d) $L^L_{max} = max(\kappa^{sym}_{max})/\sqrt{EKE}$ (km) between 500m and 800m depth.

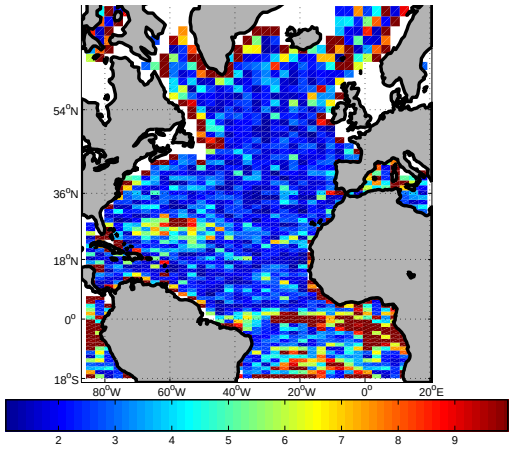

(e) The ratio $max(\kappa^{sym}_{max})/max(\kappa^{sym}_{min})$ between 500m and 800m depth.

Figure 14: $z \approx -650m$

4 Discussion

In the final part of this thesis we summarize the results and relate it to some previous studies.
Diffusion is the commonly used model for representing eddy-induced passive tracer transport in Ocean General Circulation Models (Berloff & McWilliams, 2002), although its usefulness has been questioned by many authors (e.g. Davis (1987), Berloff & McWilliams (2002)). One problem associated with eddy diffusivity modelling is that the components of the diffusivity tensor do not converge to a constant value within a short time lag. A slow convergence of the diffusivity tensor is caused by the slow memory loss of velocity fluctuations induced by mesoscale structures. Eddy diffusivity modelling is only appropriate if the tracer field is not changed substantially by the mean flow during an interval in which sequential particle displacements are statistically independent from each other (see Berloff *et al.* (2002), Berloff & McWilliams (2002) and Berloff & McWilliams (2003) for an up-to-date discussion of the problem).
In this work we analyze the timeseries of κ^{sym} up to a lag of 60 days, although previous studies suggest that κ^{sym} does not reach an asymptotic value within this period. We choose to restrict our study to the 60-day length for two reasons: Most importantly, the computational method we use forces us to compromise statistical accuracy if longer lags are analyzed. Furthermore, since our analysis aims to be of relevance for flux-gradient parameterizations of unresolved transport in ocean-components of climate models, the time-interval for which statistical transport properties are to be analyzed is bounded by properties of mean-advection. We think that two months can be regarded as a reasonable timespan in oceanic flows with relatively steep mean-tracer gradients in regions with strong mean flow (e.g. western boundary currents), because eddy-diffusivity modeling only yields a correct increase of mean-tracer variance if multiple, statistically independent particle displacements occur within an interval during which the mean advection changes the tracer concentration significantly.
We use two distinct methods to infer timeseries of κ. In EXP1, we use a method which is similar to the one used by Oh *et al.* (2000). In contrast to the findings of Oh *et al.* (2000), κ^{sym}_{min} does not reach an asymptotic value during the first 60 days in our study. In EXP2, we include the high-resolution Eulerian mean field with the intention to reduce the bias caused by mean shear. The evolution of κ^{sym}_{max} in EXP1 and EXP2 differs strongly in regions with high horizontal mean shear, but in regions with no mean shear it is almost identical. Like in EXP1, the diffusivity tensor does not converge in EXP2 within the first 60 days. The difference between κ^{sym}_{max} and κ^{sym}_{min} in EXP2 is significant and their ratio is of O(1) in most regions of the ocean. We conclude that large-scale mean shear is not the only cause of an anisotropic κ_{sym} obtained from FARE-averaging. This is in agreement with the observations made by (Kamenkovich *et al.*, 2009). We observe that, in the regions which were analyzed, κ^{sym}_{min} often attains values which are not significantly different from zero within the first 60 days after deployment.
It may be insightful to compare diffusive properties along orthogonal axes other then the pair of eigenvectors. A possible explanation for an anisotropic κ_{sym} are different transport properties in zonal and meridional direction. Our results show that $max(\kappa^{sym}_{xx})$ is generally larger than $max(\kappa^{sym}_{yy})$.
LaCasce (2000) computes streamlines of the mean flow and analyzes the components of diffusivity with respect to the along- and cross-stream direction. He finds that diffusivity is more anisotropic with respect to this local coordinate frame than with respect to the zonal and meridional direction. This observation has also been made by Griesel (pers. comm.), who assessed the time series of the diffusivity tensor's components from the velocity field of a $1/10^o$ numerical model of the Antarctic Circumpolar Current. Griesel obtains timeseries with lengths of up to several years for the along- and cross stream components. She applies methods to reduce dispersion by mean shear, and notes that along-stream diffusion is several times higher than cross stream diffusion. The cross-stream component reaches a pronounced global maximum within the first 50 days and then converges to

a depth-independent value. The along-stream component increases rapidly within the first 90 days and keeps this maximal value for longer lags, showing a depth dependece also at long lags. The horizontal distribution of the two components does not seem to be correlated.
This work aimed to improve simple eddy-diffusivity parameterizations of isopycnal dispersion for coarse resolution ocean models by inferring appropriate eddy-diffusivity constants from the flow field of an eddy-permitting model. Despite the failure to find appropriate constants, which might in part be rooted in the fact that eddy-diffusivity modelling itself is inadequate, our results contribute to the understanding of the evolution of the single-particle diffusivity tensor for time lags up to 60 days.

Acknoledgements: I want to thank Professor Sarah T. Gille and Dr. Alexa Griesel, who supported my stay at Scripps Institution of Oceanography (U. C. San Diego) and gave me valuable advice relating to the topic of research. I received financial support from the Joint Office for Science Support (JOSS) of the University Corporation for Atmospheric Research (UCAR) to visit the CLIVAR WGOMD Workshop on Ocean Mesoscale Eddies in Exeter, UK. Finally I want to thank Dr. Carsten Eden, my supervisor, for patiently involving me in many interesting discussions about this topic.

References

Barnier, B., Siefridt, L. & Marchesiello, P., 1995 Thermal forcing for a global ocean circulation model using a three year climatology of ecmwf analysis. *J. Mar. Sys.* **6**, 363–380.

Berloff, P. S. & McWilliams, J. C., 2002 Material transport in oceanic gyres. part ii: Hierarchy of stochastic models. *Journal of Physical Oceanography* **32**, 797–830.

Berloff, P. S. & McWilliams, J. C., 2003 Material transport in oceanic gyres. part iii: Randomized stochastic models. *Journal of Physical Oceanography* **33**, 1416–1445.

Berloff, P. S., McWilliams, J. C. & Bracco, A., 2002 Material transport in oceanic gyres. part i: Phenomenology. *Journal of Physical Oceanography* **32**, 764–796.

Davis, R., 1983 Oceanic property transport, lagrangian particle statistics, and their prediction. *Journal of Marine Research* **41**, 163–194.

Davis, R., 1987 Modeling eddy transport of passive tracers. *Journal of Marine Research* **45**, 635–666.

Davis, R. E., 1991 Observing the general circulation with floats. *Deep Sea Res.* **38, Suppl. 1**, 531–571.

Eden, C. & Greatbatch, R. J., 2008 A diagnosis of isopycnal mixing by mesoscale eddies. *Ocean Modelling.* **27**, 98–106.

Efron, B., 1979 Bootstrap methods: Another look at the jackknife. *The Annals of Statistics* **7**, 1–26.

Einstein, A., 1905 On the movement of small particles suspended in stationary liquids required by the molecular-kinetic theory of heat. *Annalen der Physik* **17**, 549–560.

Garrett, C., 1983 On the initial streakiness of a dispersing tracer in two- and three-dimensional turbulence. *Dyn. Atmos. Oceans* **7**, 265–277.

Garrett, C., 2006 Turbulent dispersion in the ocean. *Progress in Oceanography* **70**, 113–125.

Kamenkovich, I., Berloff, P. & Pedlosky, J., 2009 Anisotropic material transport by eddies and eddy-driven currents in a model of the north atlantic. *J. Phys. Oceanogr.* p. in press.

Kundu, P. K. & Cohen, I. M., 2002 *Fluid mechanics*. Academic Press.

LaCasce, J. H., 2000 Floats and f/h. *J. Mar. Res.* **58**, 61–65.

Lee, M. M., Nurser, A. J. G., Coward, A. & de Cuevas, B., 2009 Effective eddy diffusivities inferred from a point release tracer in an eddy-resolving ocean model. *J. Phys. Oceanogr.* **39**, 894–914.

Oh, I. S., V., Z. & W., P., 2000 Estimating horizontal diffusivity in the east sea (sea of japan) and the northwest pacific from satellite-tracked drifter data. *J. Geophys. Res.* **105(C3)**, 6483–6492.

Pacanowski, R. C., 1995 Mom 2 documentation, user's guide and reference manual. technical report, gfdl ocean group, gfdl, princeton, usa. .

Rhines, P. & Schopp, R., 1996 The wind-driven circulation: Quasi- geostrophic simulations and theory for nonsymmetric winds. *J. Phys. Oceanogr.* **21**, 1438–1469.

Swenson, M. S. & Niiler, P. P., 1996 Statistical analysis of the surface circulation of the california current. *J. Geophys. Res.* **101**, 22631–22646.

Taylor, G. I., 1922 Diffusion by continuous movements. *Proc. London Math. Soc.* **20**, 196–212.